Chemical Physics Reviews

Electrochemical production of two-dimensional atomic layer materials and their application for energy storage devices

Cite as: Chem. Phys. Rev. 4, 011306 (2023); https://doi.org/10.1063/5.0134834
Submitted: 14 November 2022 • Accepted: 30 December 2022 • Published Online: 13 February 2023

Hoyoung Lee, Shikai Jin, Jiyong Chung, et al.

Chemical Physics Reviews REVIEW scitation.org/journal/cpr

Electrochemical production of two-dimensional atomic layer materials and their application for energy storage devices

Cite as: Chem. Phys. Rev. 4, 011306 (2023); doi: 10.1063/5.0134834
Submitted: 14 November 2022 · Accepted: 30 December 2022 ·
Published Online: 13 February 2023

Hoyoung Lee, Shikai Jin, Jiyong Chung, Minsu Kim, and Seung Woo Lee[a)]

AFFILIATIONS

George W. Woodruff School of Mechanical Engineering, Georgia Institute of Technology, Atlanta, Georgia 30332, USA

[a)]Author to whom correspondence should be addressed: seung.lee@me.gatech.edu

ABSTRACT

Two-dimensional (2D) atomic layer materials have attracted a great deal of attention due to their superior chemical, physical, and electronic properties, and have demonstrated excellent performance in various applications such as energy storage devices, catalysts, sensors, and transistors. Nevertheless, the cost-effective and large-scale production of high-quality 2D materials is critical for practical applications and progressive development in the industry. Electrochemical exfoliation is a recently introduced technique for the facile, environmentally friendly, fast, large-scale production of 2D materials. In this review, we summarize recent advances in different types of electrochemical exfoliation methods for efficiently preparing 2D materials, along with the characteristics of each method, and then introduce their applications as electrode materials for energy storage devices. Finally, the remaining challenges and prospects for developing the electrochemical exfoliation process of 2D materials for energy storage devices are discussed.

TABLE OF CONTENTS

I. INTRODUCTION

Two-dimensional (2D) materials, triggered by the discovery of graphene, have been applied in a wide variety of fields over the past decade due to their superior properties. Graphene is well-known to be a paradigm of atomically thin 2D materials with exceptional mechanical, thermal, optoelectronic, and electrical properties.[1–5] The rise of graphene has greatly inspired the exploration of other classes of 2D materials, including black phosphorus, transition metal dichalcogenides (TMDs), hexagonal boron nitride (h-BN), transition metal oxides (TMOs), metal carbides or nitrides (MXenes), and covalent organic frameworks (COFs).[6–10] Outstanding properties of these 2D materials[11–15] have led to great success in applications such as energy storage devices, electrochemical sensors, and field effect transistors.[16–20] Although 2D materials have had a significant impact on a broad range of applications, industrial-level scalability and high-quality structural control are still required for commercialization.

Since Geim and Novoselov successfully isolated high-quality graphene from highly oriented pyrolytic graphite (HOPG) by micromechanical cleavage in 2004,[1] many researchers have explored a wide range of techniques for producing atomically thin nanomaterials.[21,22] Numerous 2D material production methods have been reported, which are simply categorized into two strategies: bottom-up and top-down. Bottom-up techniques such as epitaxial growth,[23–28] chemical or hydrothermal/solvothermal synthesis,[29–34] molecular beam epitaxy,[35–39] and chemical vapor deposition (CVD)[40–43] build monolayer or few-layered sheets starting from molecular precursors. In general, 2D materials synthesized by bottom-up techniques have large grain sizes and high quality.[44–48] However, bottom-up synthetic procedures typically require expensive equipment operating under harsh conditions (e.g., high temperature and pressure) and have difficulties in

transferring samples to other substrates for post-synthesis processing. On the other hand, top-down methods such as mechanical cleavage with scotch tape, wet chemical oxidation, liquid-phase sonication, and electrochemical exfoliation are based on exfoliation from bulk crystals or powders.[1,49–52] The different bond strength between weak Van der Waals interactions along the adjacent plane and strong covalent bonds along the basal plane atoms enables layer-by-layer extraction by external force or intercalation. Mechanical exfoliation can achieve high-quality 2D materials on small scales that limit their use on a laboratory scale for fundamental study. Wet chemical oxidation and liquid-phase sonication assisted by sheer forces are facile and cost-effective methods to generate solution-processable 2D materials.[53–56] However, such processes are typically time-consuming, often employ hazardous chemicals, and provide limited control over the structure of the resulting 2D materials.[8,50,55,57]

Electrochemical exfoliation, a top-down strategy, enables efficient and large-scale production of 2D materials while maintaining high quality comparable to those produced from bottom-up techniques. This process is based on a collective phenomenon consisting of ion intercalation, chemical oxidation or reduction, gas evolution, mechanical expansion, and exfoliation. Various ions under an electric field can intercalate into most types of bulk-layered materials to reduce intermolecular interactions between layers, and subsequent gas evolution from the co-intercalated solvent molecules causes expansion and exfoliation of the 2D materials.[58,59] These processes take only several minutes to hours to synthesize solution-processable 2D materials. The electrochemical exfoliation method enables sophisticated control over the exfoliated materials by utilizing electromotive forces compared to other chemical or mechanical driving forces for exfoliation, which is a significant advantage for 2D materials used in electronic devices where structural integrity is a critical factor. In addition, this method involves various processing parameters (i.e., quality of starting materials, concentration and types of anions or cations, solvents, voltage, and time). Because of these advantages, 2D materials produced by electrochemical exfoliation have been used in a variety of applications, such as electrocatalysts,[60–63] batteries,[64–68] supercapacitors,[69–72] sensors,[73–76] passivation layer,[77] and organic field-effect transistors.[78,79] In this review, we introduce several types of electrochemical exfoliation setups and discuss the exfoliation mechanism along with examples of graphene and other 2D materials such as MoS_2 and black phosphorus. We then introduce how electrochemically exfoliated 2D materials can be used as electrode materials in various energy storage devices. Finally, we discuss the various challenges and emerging opportunities for the electrochemical exfoliation process of 2D materials for energy storage applications.

II. ELECTROCHEMICAL EXFOLIATION

A typical setup for an electrochemical exfoliation process includes a working electrode (WE), which is the bulk materials to be exfoliated, a counter electrode (CE), which is usually a metal plate or wire, a reference electrode (RE), an electrolyte, and a power supply [Fig. 1(a)]. During the exfoliation process, a fixed potential or electrical current causes the guest ions in the solvent to move into the space between the layers of the 2D material. Depending on the potential applied to the working electrode, the guest ions can be anions with a positive potential (anodic exfoliation) or cations with a negative potential (cathodic exfoliation). In general, anodic exfoliation is advantageous for producing 2D materials with high yields, exhibits high exfoliation efficiency, and is accompanied by functionalization of the products by oxidation (i.e., halide ions,[65] organic compounds,[80,81] nonmetals,[82–86] metals,[87] and metal oxides[69]), whereas cathodic exfoliation can produce high-quality 2D materials but with a relatively low rate.[88,89] In addition, a dual exfoliation technique has been developed to simultaneously exfoliate 2D materials from both the cathode and anode [Fig. 1(b)].[90,91] Bipolar exfoliation [Fig. 1(c)] has recently been highlighted as a method that enables facile and scalable manufacturing of 2D materials.[92–94] A wireless exfoliation process via a redox reaction allows the use of small powders or flakes as starting materials. A bipolar electrode (BE) is placed in between two metallic feeder electrodes (FE), and the exfoliation process takes place in the absence of direct

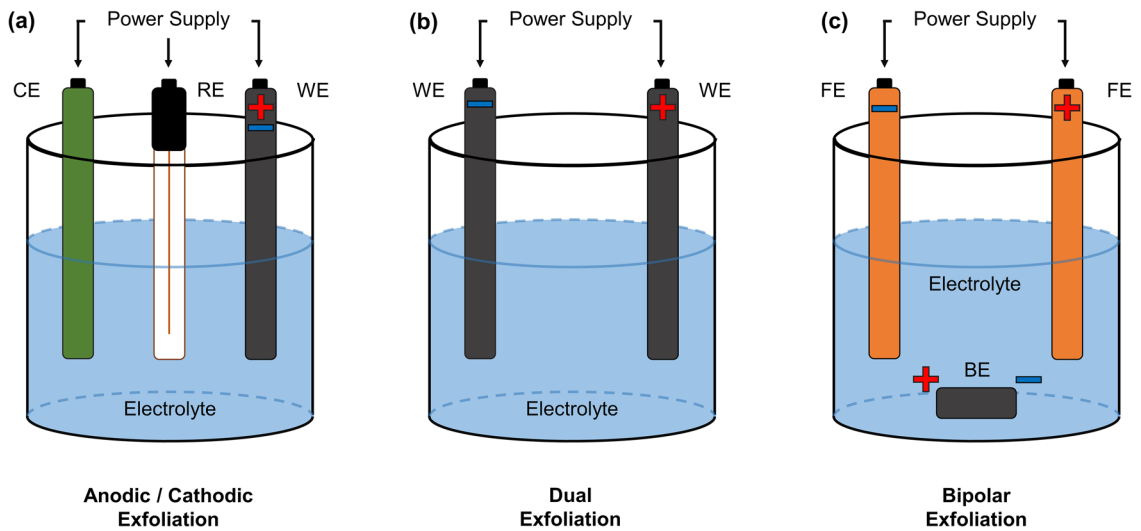

FIG. 1. Schematic illustrations of (a) anodic/cathodic, (b) dual, and (c) bipolar electrochemical exfoliation setups.

Ohmic contact, unlike the previously mentioned processes, which require direct contact of all components.

A. Anodic exfoliation

Anodic exfoliation drives the intercalation of negatively charged anions into the 2D material at the working electrode in aqueous or organic solvent conditions (Table I). The first attempt at electrochemical exfoliation was demonstrated by anodic exfoliation of graphite in ionic liquids.[95] Wang and co-workers applied a constant voltage of 5 V to two graphite rods as both the anode and cathode in 0.001 M poly(sodium-4-styrenesulfonate) (PSS) aqueous solution, and after 20 min, a black-colored graphene product began to appear.[95] In this process, polystyrenesulfonate anions act as both intercalants and surfactants.[95] Subsequently, Su *et al.* demonstrated electrochemical exfoliation of HOPG and natural graphite flakes in dilute sulfuric acid (0.5 M, pH = 0.3),[96] which is inspired by the report in 1996 that the expandable graphite was produced by incorporating concentrated sulfuric acid (H_2SO_4).[97] The thickness of the graphene sheets obtained in this study was less than 3 nm thick, and the maximum dimension was 30 μm.[96] They reported that at low voltages (<10 V), the exfoliation process was slow and efficient, but at high voltages (>25 V), fast and non-uniform exfoliation was observed.[96] Feng group succeeded in fabricating a high fraction of few-layered graphene using defective graphite foils that facilitated intercalation of anions in 0.1 M H_2SO_4, and achieved high yields (over 60% of the total amount of starting graphite materials) in 2013.[78] In their study, the lateral size of the electrochemically exfoliated graphene (EG) sheet was around 10 μm with a carbon-to-oxygen (C/O) atomic ratio of 12.3.[78] Later from the same group, natural graphite flakes were electrochemically exfoliated in various aqueous inorganic salts: $(NH_4)_2SO_4$, Na_2SO_4, K_2SO_4, NH_4Cl, $NaNO_3$, and $NaClO_4$.[98] Salts containing sulfate anions (SO_4^{2-}) outperformed other anions and took only 5 min to exfoliate graphite flakes into thin graphene sheets. In particular, ammonium sulfate [$(NH_4)_2SO_4$] under neutral pH conditions exhibited high exfoliation yields of graphene (>85 wt. %) with lateral sizes up to 44 μm and a high C/O ratio of 17.2.[98]

When a sufficient voltage is applied across the electrodes, the reduction of water at the cathode generates hydroxyl ions (OH^-) and the anodic oxidation of water produces oxygen radicals (O·) in the electrolyte.[58,99] Graphite edge sites and grain boundaries are preferentially oxidized by these ions and radicals.[78] Edge oxidation causes the graphite layers to expand, providing sufficient space for sulfate ions (SO_4^{2-}) and water molecules to intercalate. Various gaseous species, such as SO_2, O_2, CO, and CO_2, can be produced by SO_4^{2-} reduction, water oxidation, and carbon corrosion.[98–100] These generated gaseous species exert sufficient shear forces on the graphite layers to overcome weak van der Waals interactions, leading to the separation and production of graphene sheets (Fig. 2).[101] The previous study has explained that the higher efficiency of sulfate ions is due to the lower standard reduction potential of SO_4^{2-} (+0.20 V) compared to other anions (0.96 V for NO_3^-, 1.36 V for Cl^-, and 1.42 V for ClO_4^-). Therefore, the favorable formation of SO_2 gas from SO_4^{2-} compared to other gases (NO or Cl_2) can cause effective exfoliation of graphite in sulfate-containing solutions. Recently, the origin of superior exfoliation efficiency with SO_4^{2-} anion was studied with the support of density functional theory (DFT) calculation and *in situ* mass spectrometer.[102] The electrochemical exfoliation of HOPG in sulfuric acid using with *in situ* mass spectrometer showed that the generation of CO_2, CO, and O_2 was associated with the oxidation of carbon and co-intercalated water molecules, but no SO_2 gas was detected during exfoliation.[102] This study suggests that the repulsive interaction between SO_4^{2-} anions and graphene sheets can promote the easy

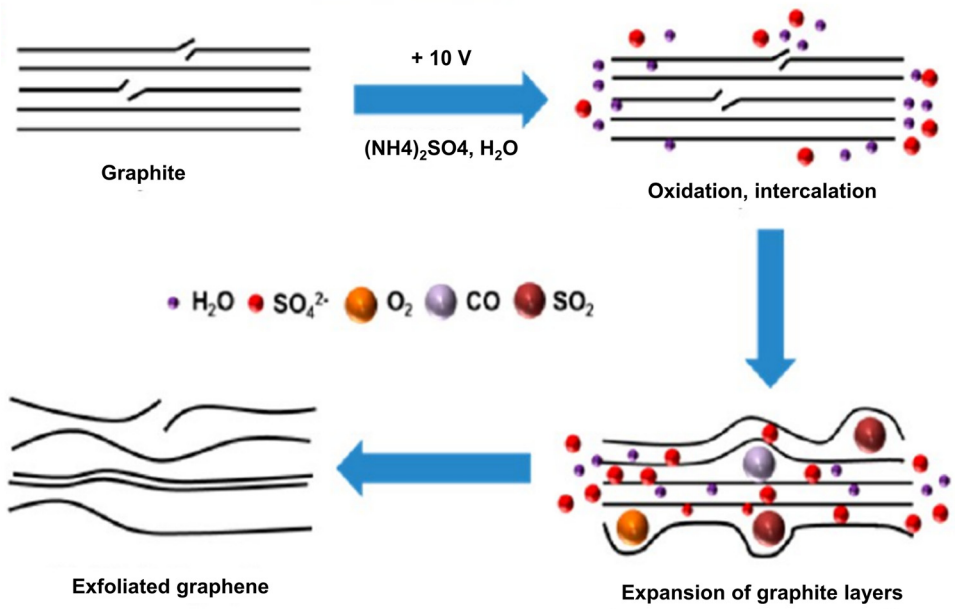

FIG. 2. Schematic illustration of electrochemical exfoliation of graphite under positive potential in sulfate-containing electrolytes. Reprinted with permission from Parvez *et al.*, J. Am. Chem. Soc. **136**(16), 6083–6091 (2014). Copyright 2014 American Chemical Society.[98]

access of sulfate anions into the graphite layers and concomitant water diffusion, thereby enhancing the exfoliation efficiency.[102]

One of the main challenges of the anodic exfoliation process is to overcome the severe oxidation of 2D materials under high positive potential. Hydroxyl and oxygen radicals can be formed by the oxidation of water as follows: $H_2O \rightarrow {}^{\bullet}OH + (H^+ + e^-) \rightarrow {}^{\bullet}O + (H^+ + e^-)$.[103] The generated radicals readily react with the graphite surface, resulting in the formation of oxygen-containing functional groups with substantial levels of defects in the exfoliated graphene.[99] Therefore, several strategies have been attempted by adding reducing agents as additives to prevent oxidative damage during electrolysis. Yang *et al.* tested a series of reducing agents (2,2,6,6-tetramethylpiperidine-1-yl)oxyl (TEMPO), ascorbic acid, and sodium borohydride to eliminate the effect of ${}^{\bullet}OH$ radicals.[103] The authors explained that the favorable reaction of ${}^{\bullet}OH$ radicals to TEMPO than the graphite reduces the oxygen content of exfoliated graphene, therefore achieving a C/O ratio of 25.3 with relatively low defects.[103] In 2015, Chen and co-workers produced graphene with a C/O ratio of 26 by adding melamine into a dilute sulfuric acid solution.[104] During the exfoliation process, melamine was adsorbed onto the graphene sheets and acted as a protective layer preventing further oxidation.[104] The authors emphasized that the graphite powder with melamine additive can improve scalable production of graphene by combining electrochemical reaction and *in situ* extraction method.[104] Ejigu *et al.* tested transition metal ions (e.g., Co^{2+}, Fe^{3+}, Ru^{3+}, Mn^{2+}, Ir^{3+}, and Sn^{4+}) as catalytic antioxidant additives during the electrochemical exfoliation of graphite.[69] The addition of $CoSO_4$ to the exfoliation solution achieved a graphene product with a high C/O ratio of 36. The authors proposed that the Co^{2+} is oxidized to Co^{4+} at the graphite surface and acts as an active electrocatalyst for O_2 evolution. As a result, the deposited Co^{4+} cations could prevent the oxidation of graphite by ${}^{\bullet}OH$ radicals.[69]

The aqueous phase anodic exfoliation process has been applied to the production of other 2D materials. For example, You *et al.* first demonstrated anodic exfoliation of MoS_2 in 0.5 M H_2SO_4 solution.[115] A two-electrode system was employed with a natural MoS_2 bulk crystal as the anode and a platinum (Pt) wire as the ground electrode.[115] A static bias of +1 V was applied to the MoS_2 crystal for 10 min, and the potential was increased to +10 V for 30 min to complete the exfoliation process.[115] The obtained MoS_2 nanosheets had a lateral dimension of ~10 μm and a high degree of crystallinity.[115] Later, the same group prepared MoS_2 nanosheets with a larger lateral size (~50 μm) and a lower degree of oxidation in 0.5 M Na_2SO_4 aqueous solution.[116] From an industrial point of view, it is preferable to use inexpensive bulk MoS_2 powders as a starting material rather than expensive bulk crystals. Wu *et al.*, therefore, employed MoS_2 powder as the starting material to fabricate few-layered MoS_2 nanosheets.[122] The MoS_2 powder was suspended in 1 M Na_2SO_4 aqueous solution by sonication for 60 min and poured into a polypropylene membrane bag (125 000 mesh) with titanium mesh (100 mesh).[122] Defect-rich MoS_2 nanosheets were obtained under a constant voltage of 20 V for 4 h, followed by a post-treatment of tip sonication for 2 h.[122] Recently, Pan *et al.* reported a new electrochemical strategy demonstrating fast conversion from bulk MoS_2 to bi/tri-layer MoS_2 [Figs. 3(a)–3(e)].[123] Due to the intrinsic layer-dependent valence band of MoS_2, the valence bands of

TABLE I. Reported anodic exfoliation systems of 2D materials. Note: PSS: poly(sodium-4-styrenesulfonate); SDBS: sodium dodecyl benzene sulfonate; TSCuPc: copper phthalocyanine-3,4′,4″,4‴-tetrasulfonic acid tetrasodium salt; 9-ACA: 9-anthracene carboxylate; [C_8mim]: 1-octyl-3-methyl-imidazolium; [BMIm]: 1-butyl-3-methylimidazolium.

Working electrode	Salt	Solvent	Voltage	Thickness	Ref.
Graphite rod	PSS	H_2O	5 V	1–2 layers	95
Graphite rod	SDBS	H_2O	25 V	···	105
Graphite rod	TSCuPc	H_2O	12 V	1–6 layers	106
Graphite rod	9-ACA and NaOH	H_2O	20 V	0.79 nm	107
Graphite rod	$[C_8mim][PF_6]$	H_2O	15 V	1.1 nm	108
HOPG and graphite rod	[BMIm][BF_4]	H_2O	1.5–15 V	···	58
HOPG and graphite flake	H_2SO_4 or K_2SO_4	H_2O	10 V	1–7 layers	96
Flexible graphite paper	H_2SO_4	H_2O	1.6–5 V	<3 layers	109
Graphite flake	$(NH_4)_2SO_4$ or Na_2SO_4 or K_2SO_4	H_2O	10 V	1–2 layers	98
Graphite foil	H_2SO_4 or Na_2SO_4 or $LiClO_4$	H_2O	10 V	6–8 layer	110
Graphite foil	$NaBF_4$	H_2O	10 V	<3 layers	111
Graphite rod	NaOH and H_2O_2	H_2O	3V	3 layers	112
Graphite flake	H_2SO_4	H_2O	10 V	1–3 layers	78
Graphite foil	NaOH and Na_2SO_4	H_2O	3–10 V	2–4 layers	113
Graphite foil	TBA·HSO_4	H_2O	±10 V	1–3 layers	114
MoS_2 crystal	H_2SO_4	H_2O	10 V	1–3 layers	115
MoS_2 crystal	Na_2SO_4	H_2O	10 V	1–5 layers	116
BP crystal	H_2SO_4	H_2O	1–3 V	···	117
Sb crystal	Na_2SO_4	H_2O	10 V	3.5 nm	118
BP crystal	Na_2SO_4	H_2O	10 V	3–4 layers	119
Bi_2Se_3 and Bi_2Te_3	Na_2SO_4	H_2O	±10 V	···	120
Ti_3AlC_2	NH_4Cl, TMA·OH	H_2O	5 V	1–2 layers	121

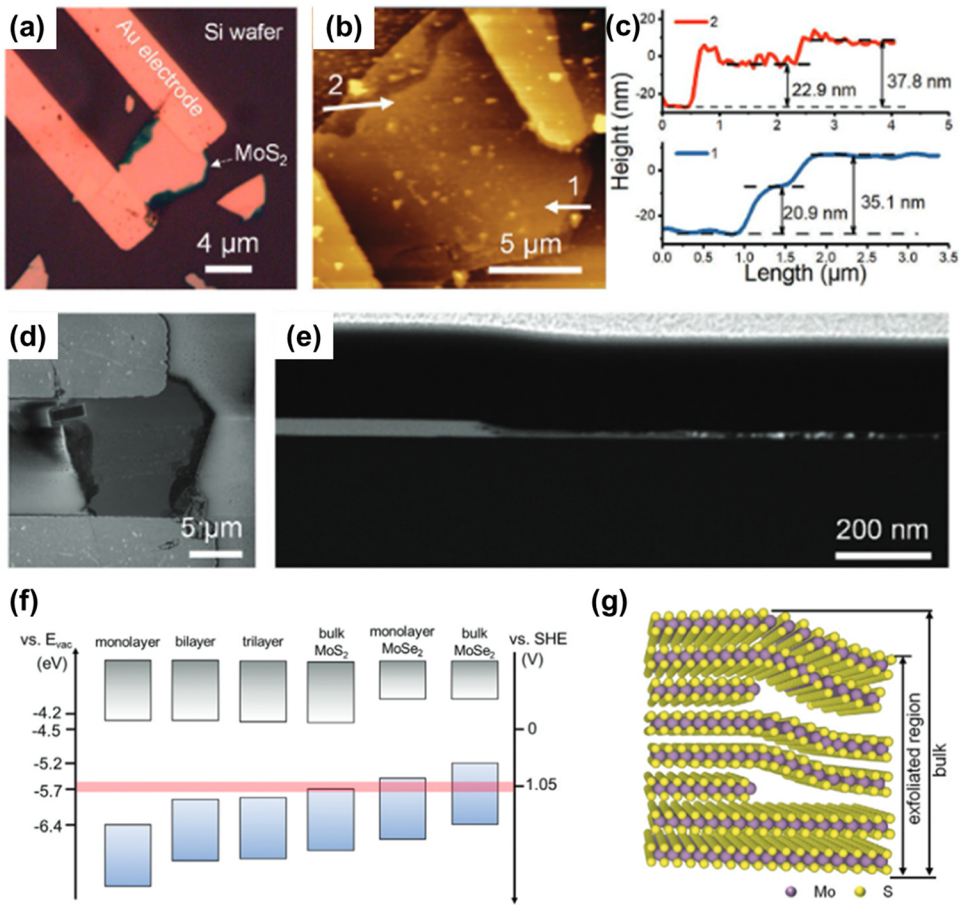

FIG. 3. (a) Optical image of MoS_2 sheet after electrochemical treatment. [(b) and (c)] Atomic force microscopy (AFM) image and the thickness profile. (d) The SEM image of the MoS_2 sheet. (e) Cross-profile scanning transmission electron microscopy (STEM) image of the MoS_2 sheet from the rectangle region in (d). (f) Energy band diagrams of MoS_2 and $MoSe_2$ with different layers. The red band represents the redox potential range from Refs. 124 and 125. (g) The schematic illustration of the edge and the basal plane of MoS_2 after exfoliation. Reproduced with permission from Pan *et al.*, Adv. Funct. Mater. **31**(8), 2007840 (2021). Copyright 2020 John Wiley and Sons.[123]

mono-, bi-, and tri-layer MoS_2 are lower than the oxidation potential region of Mo, where the bulk MoS_2 valence band falls into the region [Fig. 3(f)]. Therefore, only bulk MoS_2 crystal was electrochemically exfoliated into few-layered MoS_2 flakes.[123]

Black phosphorus has recently attracted scientific interest due to its excellent carrier mobility and tunable bandgap.[126] Black phosphorus not only exhibits high electric conductivity, but also has the most thermodynamically stable structure of all phosphorus allotropes and the lowest risk of explosion during chemical processes.[127–129] It consists of multiple puckered sheets of covalently bonded phosphorus atoms in a honeycomb structure and held by weak van der Waals interactions between the layers, which can be easily separated into single-layer black phosphorus, phosphorene. Ambrosi *et al.* successfully obtained black phosphorus nanosheets from bulk flakes in 0.5 M Na_2SO_4 solution via aqueous phase anodic exfoliation [Figs. 4(a)–4(c)].[117] A positive DC voltage of +1 V was first applied to the black phosphorus crystal for 2 min; then, the voltage was increased to +3 V to intercalate the anion species (SO_4^{2-}) into the interlayer of the bulk crystal, causing it to expand and exfoliate over time.[117] The reduced thickness of black phosphorus was observed with scanning transmission electron microscopy (STEM) image, and high-resolution x-ray photoelectron spectroscopy (XPS) spectra of the P 2p signal confirmed the oxidation of the exfoliated nanosheets [Figs. 4(d)–4(e)].

Electrochemical exfoliation has been demonstrated to overcome metallic bonds between layered MAX nanosheets. MXenes are a new class of 2D materials discovered in 2011.[130] They are generally produced by the selective etching of A from MAX layered counterparts, where the MAX phases[130,131] as the chemical composition of $M_{n+1}AX_n$, where n = 1–3, "M" is the early transition metal (such as Sc, Ti, V, Cr, Zr, Nb, or Mo), "A" represents an IIIA or IVA group elements, and "X" is carbon and/or nitrogen. Traditionally, the A layer is etched using highly hazardous hydrofluoric acid HF or LiF/HCl solution,[132–134] which has been a major barrier to the scale-up of production and wider adoption of MXenes as functional materials. In 2017, a new attempt to synthesize MXene without fluoride-based solutions was reported. Sun *et al.* presented the first evidence of MXene without –F terminal groups using dilute aqueous HCl electrolytes.[135] They synthesized Ti_2CT_x MXene from Ti_2AlC by electrochemical exfoliation in

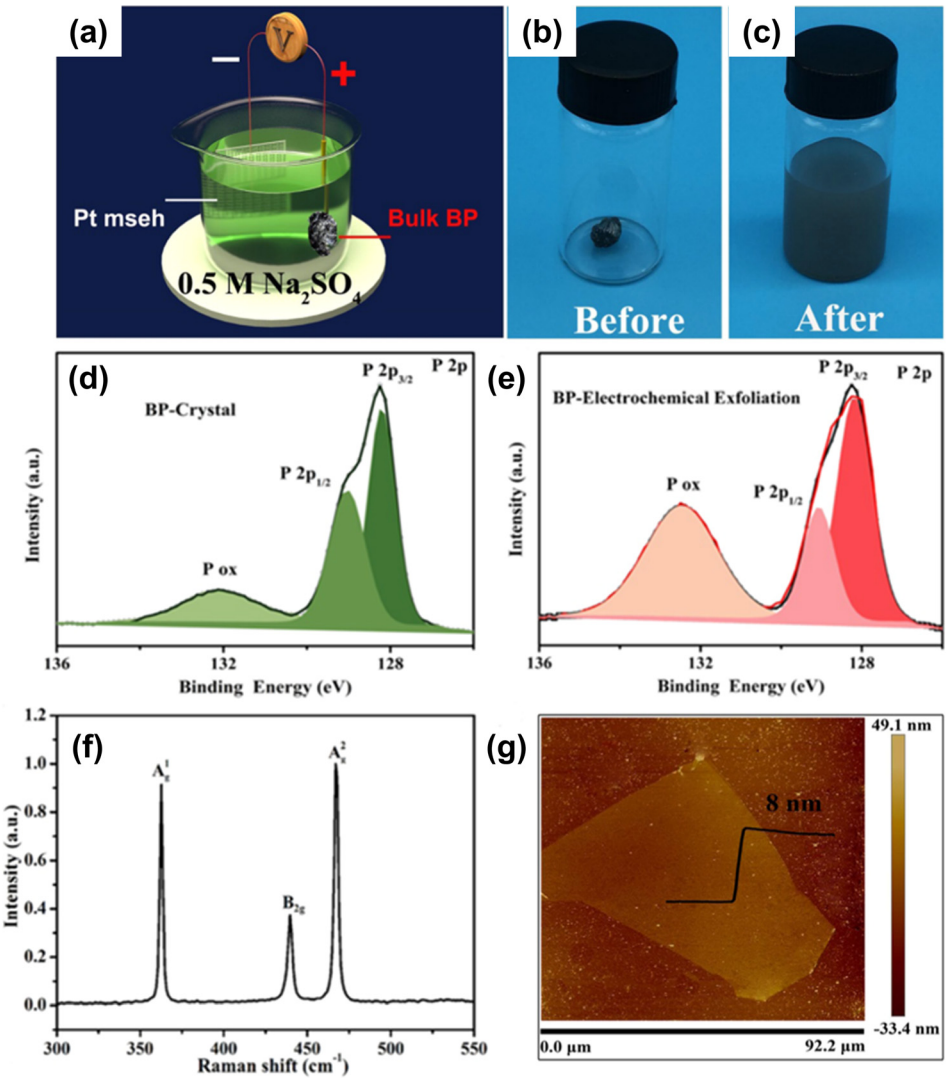

FIG. 4. (a) Schematic illustration of the electrochemical exfoliation of bulk BP into few-layered BP nanoflakes. Photographs of (b) the bulk BP crystal and (c) the electrochemically exfoliated BP nanoflakes dispersed in DMF. XPS spectra high-resolution P 2p core levels of (d) bulk BP crystal and (e) electrochemically exfoliated BP nanoflakes. (f) Raman spectrum and (g) AFM image of the electrochemically exfoliated BP nanoflakes. Reprinted with permission from Yang *et al.*, ACS Appl. Mater. Interfaces **11**(6), 5938–5946 (2019). Copyright 2019 American Chemical Society.[119]

HCl electrolyte, in which Tx represents different terminal groups such as –F, –O, and –OH. They demonstrated that Ti_2CT_x MXene produced from electrochemical exfoliation was terminated with –Cl, –O, and –OH groups, but not –F groups.[135] Recently, Yang *et al.* demonstrated fluoride-free electrochemical delamination of Ti_3AlC_2 to Ti_3C_2 in 1 M NH_4Cl and 0.2 M tetramethylammonium hydroxide (TMA·OH).[121] Two pieces of bulk Ti_3AlC_2 were used as anode and cathode, respectively, and chloride ions in the electrolyte selectively etched Al under constant potential of (+5 V) for 12 h.[121] Yin *et al.* reported the synthesis of Ti_3C2F_x MXene using compact Ti_3AlC_2 bulk as starting material via a sealed three-electrode electrochemical etching system.[136] During the electrochemical process, the F anions in the nonaqueous [BMIM][PF_6] electrolyte reacted with the Al atoms.[136] After 5-h exfoliation, $Ti_3C_2F_x$ sheets with an average lateral size of 350 ± 27 nm and height profiles of two $Ti_3C_2F_x$ sheets showed thickness values of 2.5 and 3 nm were synthesized.[136] In addition, the degree of fluorination of as-prepared $Ti_3C_2F_x$ MXene with CF and TiF_3 was controlled by adjusting the etching potential.[136]

B. Cathodic exfoliation

Anodic exfoliation enables an efficient 2D material production process with high production rates, but oxidation of the exfoliated product is unavoidable. This can be a major drawback if certain applications, such as electronics, require pure 2D materials with no surface oxidation. To preserve the intrinsic characteristics of 2D materials,

cathodic exfoliation is a promising route as a non-oxidative exfoliation process as it applies a negative potential to the layered material for the intercalation of negatively charged ions (Table II).

In a rechargeable lithium-ion battery (LIB) system, Li^+ ions are reversibly intercalated into the graphite anode, which is the lithium host.[137] During charging/discharging, co-intercalation of solvent causes loss of reversibility and severe volume changes of graphite electrode. Such expansion of the graphite electrode in the battery system leads to undesirable exfoliation of the graphite. Inspired by this phenomenon, Wang *et al.* reported the cathodic exfoliation of graphite in a non-aqueous electrolyte consisting of $LiClO_4$ and propylene carbonate (PC).[59] Co-intercalation of PC solvent with Li^+ (Li^+:2PC and Li^+:3PC) was observed at high potentials of -15 ± 5 V. The expanded graphite was then washed with acid and water to separate the individual layers with the aid of hydrogen gas evolution ($Li + 2H_2O \rightarrow 2LiOH + H_2$).[59] Zheng *et al.* prepared semiconducting 2D materials such as MoS_2, WS_2, TiS_2, TaS_2, and ZrS_2 by controlling the lithiation and sonication processes of the intercalated compounds in the aqueous phase.[138] The lithiation process was performed in a battery test system using a Li foil anode as a Li-ion source. After the lithium intercalation process using galvanostatic discharge at a current density of 0.05 mA, the Li-intercalated 2D materials were washed with acetone and ultrasonicated in water for further exfoliation process.[138] In 2018, few-layered silicene nanosheets were also obtained by the successive electrochemical lithiation and delithiation processes.[139] First, the lithiation of Si nanopowders was performed in Li-ion coin cells by a discharging process. Subsequent delithiation by rinsing with de-ionized water or isopropyl alcohol produced graphite-like "siliphite" or few silicene layers, respectively.[139] The authors claimed that different exfoliation phenomena were due to different delithiation kinetics depending on proton concentration.[139]

As an alternative to small Li^+ ion (diameter: ~0.18 nm), tetraalkyl ammonium (TAA^+) cations with larger sizes such as tetramethylammonium (TMA^+, diameter: ~0.558 nm), tetra-etyl-ammonium (TEA^+, diameter: ~0.674 nm), and tetra-n-butyl-ammonium (TBA^+, diameter: ~0.826 nm) have been used as intercalating agents for cathodic intercalation. Zhong and Swager first demonstrated the two-step intercalation of Li^+ and TBA^+ into graphite.[140] Graphite was first expanded by smaller-sized Li^+ ions and then significantly expanded by replacing the Li^+ ions with larger TBA^+ cations. Later, Yang *et al.* studied the electrochemical exfoliation of graphite rod and HOPG in TBA^+-containing electrolytes with various organic solvents such as acetonitrile (AN), N,N-dimethylformamide (DMF), and propylene carbonate (PC).[141] The authors suggested that effective graphite exfoliation was obtained by both intercalation of solvated cations into graphite and subsequent gas bubbling from the decomposition of the electrolyte. Cooper *et al.* compared exfoliation efficiency of HOPG with quaternary ammonium cations with different sizes: TBA^+, TEA^+, and TMA^+.[142] TBA^+ cation was found to be the most effective for HOPG expansion, followed by TEA^+. However, a sonication step was generally required to split the graphite layers uniformly. Recently, Zhang *et al.* improved exfoliation efficiency by employing a sandwich-structured electrode that can promote uniform cation intercalation into graphite.[143] The authors also tested the electrochemical exfoliation of graphite with various organic electrolytes consisting of TAA^+ salts in different aprotic polar solvents (acetone, DMF, NMP, DMSO, AN, and PC) to investigate the effects of cations and solvent molecules solvation on the exfoliation process.[143] Electrochemical intercalation of TBA^+ in propylene carbonate exhibited a high exfoliation yield (91.5%) of few-layered (>80%, 1–3 layers) graphene at high speed (over 50 g h^{-1}).[143] The authors suggested that the size of the solvated TAA^+ ions rather than the size of the bare cations affects the efficiency of intercalation and thereby the exfoliation of graphite.[143]

In addition to graphene, Yang *et al.* demonstrated successful electrochemical delamination of bulk BP crystal into few-layered BP flakes with high yields (up to 78%) using quaternary ammonium molecules as intercalating agents [Figs. 5(a) and 5(e)].[144] In this study, 0.1 M tetra-n-butyl-ammonium bisulfate ($TBA{\cdot}HSO_4$) in anhydrous PC solvent was used as an electrolyte and a constant potential of −8 V was applied.[144] The authors proposed three key factors for effective intercalation and exfoliation: (1) the variable vertical diameter of flexible n-butyl chains (0.47–0.89 nm) matches the interlayer distance of BP (0.53 nm); (2) the penetration and reduction of solvated protons ($HSO^{4-} \rightleftharpoons SO_4^{2-} + H^+$, $2H^+ + 2e \rightarrow H_2$) further increase the distance between two adjacent BP layers; (3) the solvent (propylene carbonate) stabilizes the exfoliated flakes against re-aggregation [Fig. 5(d)].[144] Later, Li *et al.* reported ultrafast cathodic expansion (less than 1 min) of bulk BP employing TBA^+ as a cationic intercalant in polar aprotic solvents such as dimethyl sulfoxide (DMSO).[145] In addition to BP, TBA^+ cations (0.05 M) dissolved in propylene carbonate (PC) have been used to demonstrate cathodic exfoliation of 2D transition metal dichalcogenide superconductors (2DSCs) such as $Nb(Se/Te)_2$, $Ta(S/Se)_2$, $Ti(S/Se)_2$, and $MoTe_2$.[146]

Considering the scalability and cost of the electrochemical exfoliation process, it is more reasonable to employ environmentally benign aqueous electrolytes instead of expensive and often toxic organic solvents. Dalal *et al.* demonstrated cathodic exfoliation of graphite foils using various aqueous solutions containing varying concentrations of alkali metal chloride salts (LiCl, NaCl, KCl, RbCl, and CsCl).[147] Sufficiently high cathodic voltages (−10 V and above) and high concentrations of cations (2 M and above) were required to achieve cation intercalation and subsequent hydrogen gas evolution processes.[147] Graphene nanoplatelets (mainly 10–13 layer graphene sheets) generated from the KCl aqueous electrolyte in a short period of time (<10 min) exhibited low-defect densities (I_D/I_G of 0.06, a C/O ratio of 57.8) and high exfoliation yields (>80%).[147] Garcia-Dali and co-workers also reported the successful use of aqueous alkali metal electrolytes (most notably, 4 M KCl) for cathodic delamination of MoS_2 [Fig. 6(a)].[148] A fast and efficient cathodic exfoliation was achieved using an aqueous solution, and moreover, the electrochemical route prevented oxidation [Figs. 6(h)–6(j)] or phase transformation of the exfoliated products [Figs. 6(b)–6(g)].[148]

C. Dual exfoliation

The simultaneous exfoliation process at both working and counter electrodes within a single electrochemical cell can improve the energy utilization of electrochemical exfoliation and increase the production rate of 2D materials. Mao and co-workers demonstrated a graphite–graphite cell in a protic ionic liquid (PIL) for simultaneous intercalation/exfoliation on both electrodes with an additional shear grinding process.[157] Highly expanded graphite at the cathode and fully oxidized graphite at the anode were obtained at a cell voltage of 3 V,

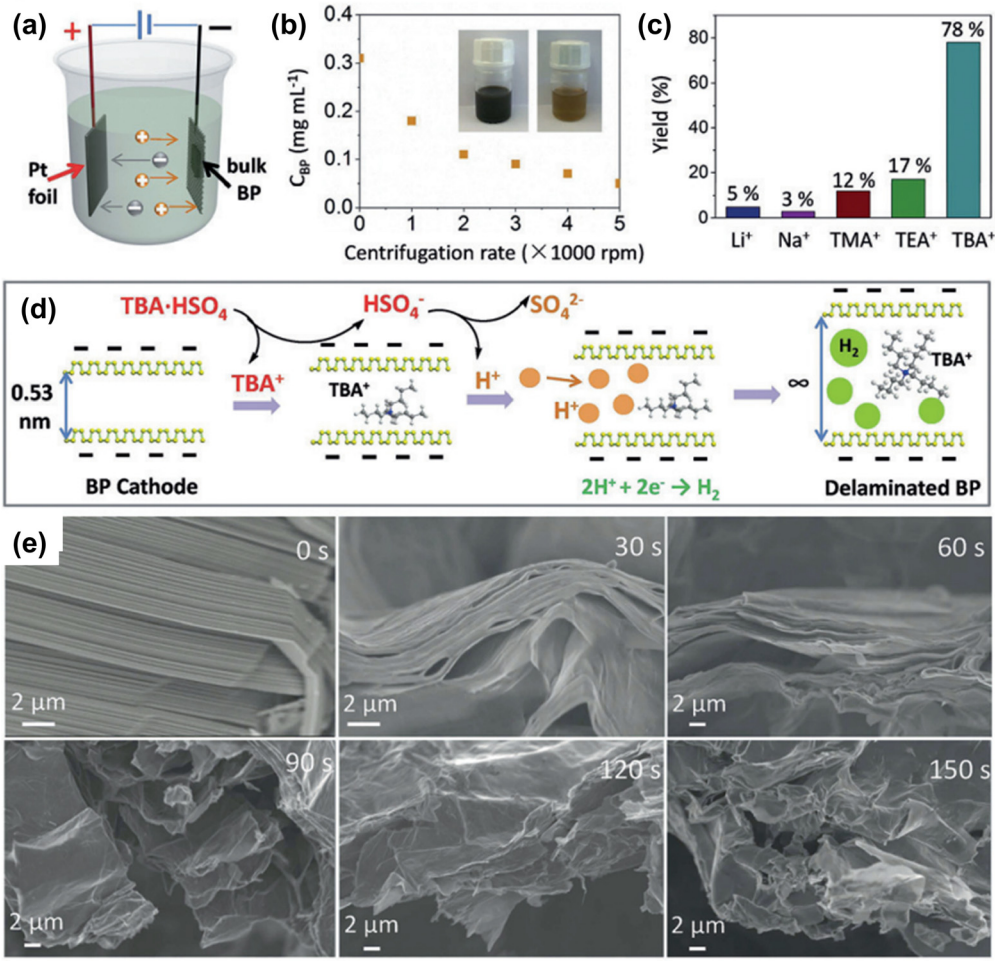

FIG. 5. (a) Schematic illustration of the reaction cell. (b) Centrifugation rate as a function of the concentration of BP dispersion in isopropyl alcohol. Inset: the BP dispersion (left); the BP dispersion after centrifugation (right). (c) The delamination yields depending on the intercalating cations. (d) Schematic illustration of the mechanism for the intercalation process. (e) SEM image of the BP cathode after various periods of intercalation. Reproduced with permission from Yang *et al.*, Angew. Chem. Int. Ed. **57**(17), 4677–4681 (2018). Copyright 2018 John Wiley and Sons.[144]

and mechanical grinding was performed to separate the graphene sheets.[157] Yang *et al.* achieved dual intercalation/exfoliation in both graphite foils using alternating current in 0.1 M tetra-n-butylammonium bisulfate (TBA·HSO_4) aqueous solution.[114] High exfoliation efficiency (80% total yield, 75% of graphene is composed of 1–3 layers) was achieved with ultra-high production capacity (over 20 g h^{-1}), and exfoliated graphene showed remarkable hole mobility up to 430 cm^2 V^{-1} s$^{-1.114}$ Later, Zhang and Xu developed an electrode design for high-yield, scalable dual-electrode exfoliation using $TBAClO_4$/PC solution, where TBA^+ and ClO_4^- can simultaneously intercalate into both the graphite cathode and anode, respectively [Fig. 7(a)].[90] The authors designed graphite electrodes wrapped in a confined space between porous metal meshes for both anode and cathode,[90] which allows sufficient intercalation of both cations and anions. As a result, high yields (85% from the cathode and 48% from the anode) of few-layered graphene (>70% for 1–3 layers) were achieved at ultrahigh production rates (<25 g h^{-1}) [Figs. 7(b)–7(i)].[90]

D. Bipolar exfoliation

The recently introduced bipolar exfoliation method generally involves two feeder electrodes (FEs) that are connected to a power supply, and a bipolar electrode (BE) placed in between the two FEs [Figs. 1(c) and 8(a)]. The voltage applied across the FEs (E_{tot}) generates an electric field in the solution that induces an electric potential (E_{elec}) across the BE, leading to electrochemical reactions at the poles of the BE.[158–160] Crooks,[161] Duval, and co-workers[162–164] suggested that the equilibrium potential (ΔE_{elec}) can be estimated by the parameters including the distance separating the driving electrodes ($l_{channel}$), and the length of the BE (l_{elec}) and the driving total electric field (E_{tot}) as the following equation:

$$\Delta E_{elec} = E_{tot}\left(\frac{l_{elec}}{l_{channel}}\right).$$

The apparent potential difference between the opposite ends induces the asymmetric Faradaic reactions at the anodic pole and the

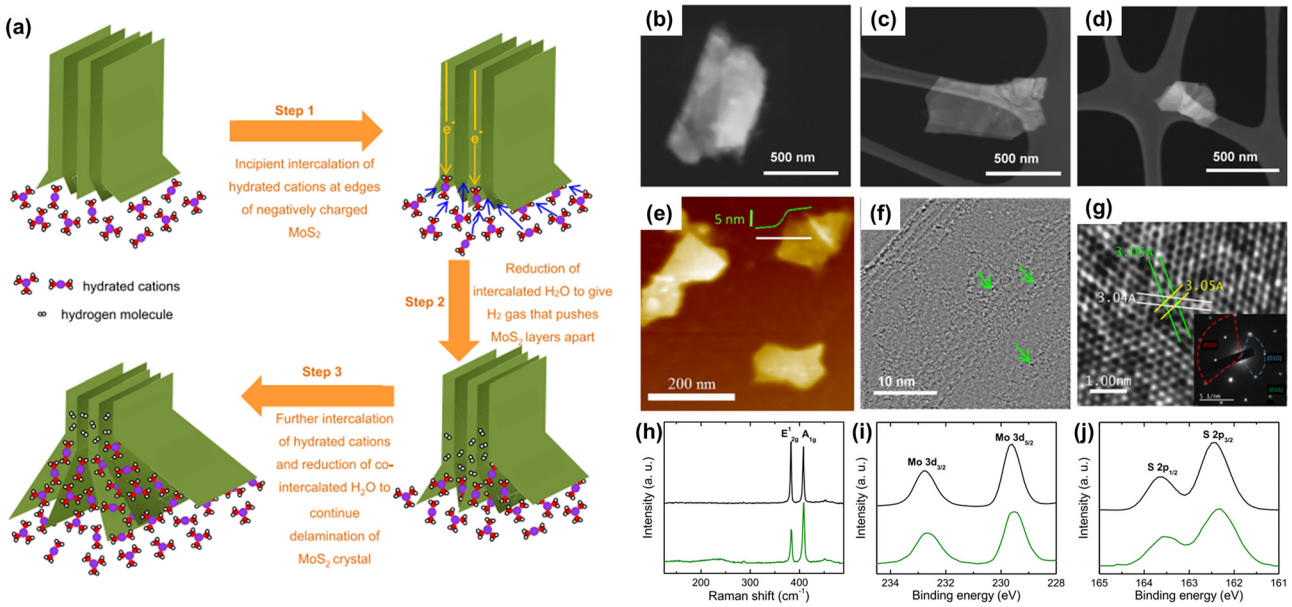

FIG. 6. (a) Schematic illustration of the cathodic delamination of MoS_2 in aqueous alkali metal-based electrolytes. [(b)–(g)] Microscopic characterization of MoS_2 cathodically exfoliated in 4 M KCl aqueous solution. [(b)–(d)] STEM, (e) AFM, and [(f) and (g)] HR-TEM images of MoS_2 nanosheets. (h) Raman spectra of the MoS_2 nanosheets. XPS spectra of high-resolution (i) Mo 3d and (j) S 2p core levels of cathodically exfoliated and bulk MoS_2 nanosheets. Reprinted with permission from Li *et al.*, Nat. Mater. **20**(2), 181–187 (2021). Copyright 2019 American Chemical Society.[146]

reduction at the cathodic pole. Implementing this principle, Allagui *et al.* reported a single-step, single-cell preparation for exfoliating and depositing partially reduced graphene oxide using bipolar electrochemistry.[165,166] In these studies, a graphite rod was placed between two stainless steel FEs in a low-conductivity solution.[165] A static voltage of 15 V cm^{-1} was set between the stainless steel FEs spaced 3 cm apart.[165] The electric field induced a potential difference of 9 V across the two ends of the graphite substrate, sufficient to promote coupled redox reactions at both the cathodic and anodic poles.[165] The authors achieved the rGO films on the positive side of stainless steel by

TABLE II. A summary of cathodic exfoliation. Note: TMA: tetramethylammonium; TEA: tetraethylammonium; TBA: tetrabutylammonium; BMPTF2N: N-butyl, methylpyrrolidinium bis(trifluoromethylsulfonyl)imide; MeCN: acetonitrile; THA: tetraheptylammonium.

Working electrode	Salt	Solvent	Voltage	Thickness	Ref.
HOPG	$LiClO_4$	PC	-15 ± 5 V	1–5 layers	59
Graphite foil	$LiClO_4$	PC	−5V	1–5 layers	140
Graphite rods	NaCl, thionin acetate	H_2O/DMSO	5 V	∼7 layers	149
HOPG	TMA·ClO_4, TEA·BF_4, TBA·BF_4	NMP	−5 V (vs. $Ag/AgClO_4$)	2–5 layers	142
HOPG, graphite rod	$BMPTF_2N$	⋯	15–30 V	2–5 layers	150
HOPG	TBA·ClO_4	DMF/MeCN	−2.2–−2.8 V (vs. Ag/Ag^+)	1–2 layers	151
MoS_2 crystals	THA·Br	MeCN	−5–−10 V	3.8 ± 0.9 nm	152
MoS_2 crystals	TBA·HSO_4	PC	−5 V	6–10 layers	153
VSe2 crystals	TPA·Cl	PC	−4–−2 V	1–5 layers	154
Sb crystals	Na_2 SO_4	H_2O	−10 V	3.5 nm	118
Sb crystals	Na_2SO_4	H_2O	−6 V	31.6 nm	155
$NiPS_3$ crystals	TBA·BF_4	DMF	−3 V	1–5 layers	82
$NbSe_2$, $NbTe_2$, TaS_2, $TaSe_2$, $TiSe_2$, and $MoTe_2$	TBA·BF_4	PC	−5 V (vs. Pt)	1–5 layers	146
BP crystals	TBA·HSO_4	PC	−8 V	3.7 ± 1.3 nm	144
BP crystals	TBA·PF_6	DMF	−5V	1–5 layers	156
BP crystals	TBA·BF_4	DMSO	−5V	5 layers	145

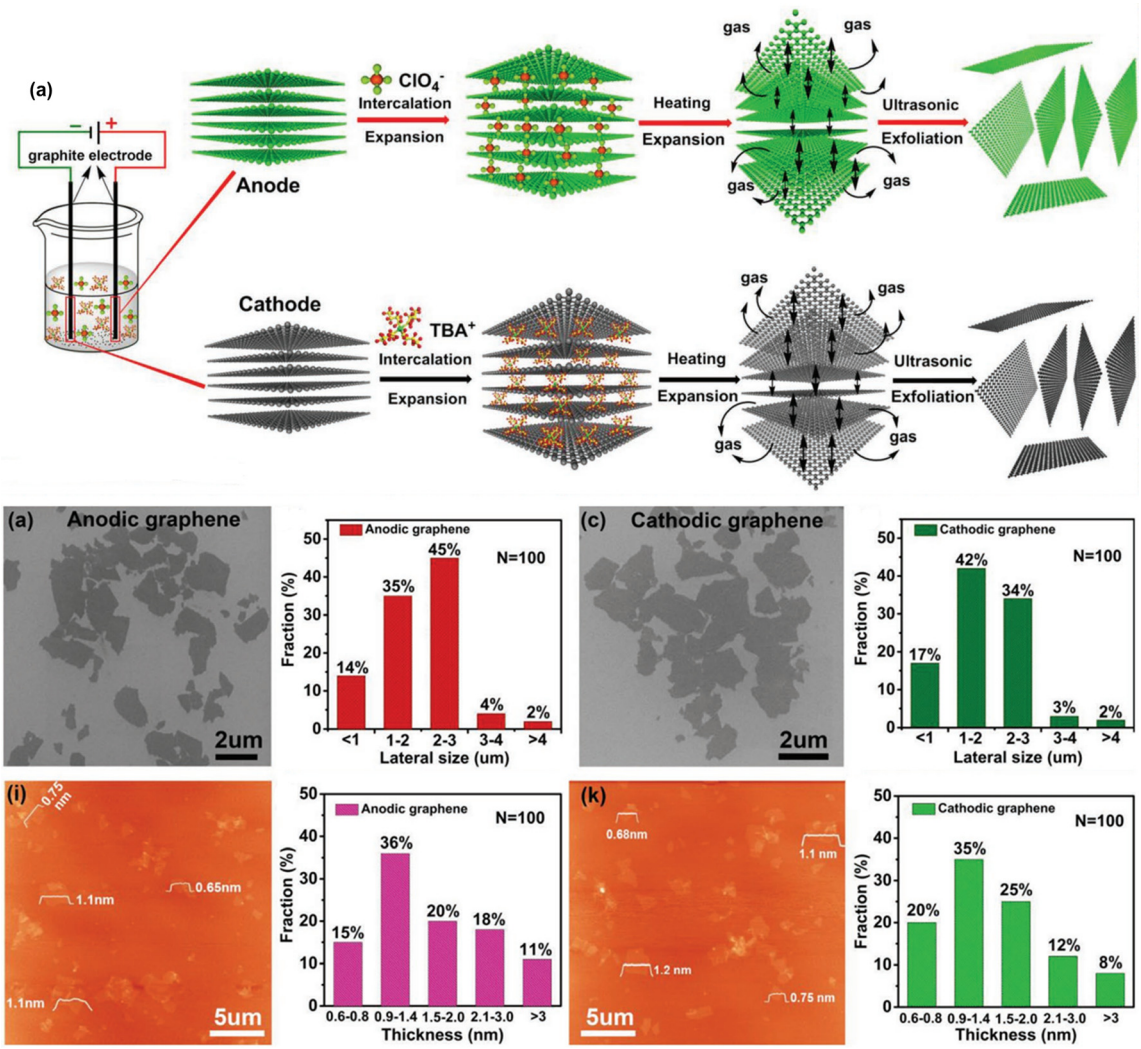

FIG. 7. Schematic illustration of dual exfoliation of graphene based on electrochemical intercalation of both anion and cation. [(b)–(i)] Morphology and thickness distribution of exfoliated graphene. Reproduced with permission from Zhang and Yu, Adv. Funct. Mater. **29**(37), 1902171 (2019). Copyright 2018 John Wiley and Sons.[90]

setting the cumulative total cell voltage limit to 15 mA h, and the thickness of the films was estimated in the nanometer range.[165] Later, the Wang group applied an apparent potential difference of 35 V on the two graphite rods as BE and successfully deposited exfoliated graphene on both the positive and negative sides of stainless steel.[167]

Unlike other electrochemical exfoliation processes that require direct electrical contact, the wireless configuration offers the ability to treat the bipolar electrode in the form of small powders, flakes, and particles. Bjerglund *et al.* first reported the bipolar electrochemical exfoliation of graphite powder with the aid of mechanical high-shear exfoliation [Figs. 8(b)–8(g) and 8(j)–8(l)].[168] The exfoliation process involved cathodic electrochemical intercalation of tetrabutylammonium ions and required an extremely high voltage of 1100 V [Figs. 8(h) and 8(i)].[168] Later, Hashimoto *et al.* also demonstrated bipolar anodic exfoliation of graphite powder at a constant current of 2450 A m^{-2}.[92] Small graphite powders (particles size 20–500 μm) were placed between two platinum FEs in dilute sulfuric acid.[92] The voltage rapidly increased at first and then settled to a steady value of ~60 V, much lower than cathodic exfoliation.[92] The exfoliation products were apparently GO nanosheets with C/O ratios of 3.6–5.3.[92]

In addition to graphite, Pumera *et al.* employed the bipolar electrochemical exfoliation process for WS_2,[63,169] black phosphorus,[170] $MoSe_2$,[171] and hexagonal boron nitride (*h*-BN) [Figs. 9(a)–9(d)].[172] The applied potential of 10 V across the Pt FEs in 0.5 M Na_2SO_4 was sufficient to induce Faradaic reactions at the surface of the electrodes, eventually leading to the exfoliation of the bulk materials into nanosheets or nanoparticles.[172] For bipolar exfoliation of *h*-BN, sodium sulfate was added as a supporting electrolyte to increase the current through the solution.[172] When the concentration of the supporting electrolyte decreases, inefficient exfoliation was observed, whereas when the concentration is increased, a damaged chemical structure of *h*-BN was obtained.[172] The h-BN nanosheets obtained in 0.5 M

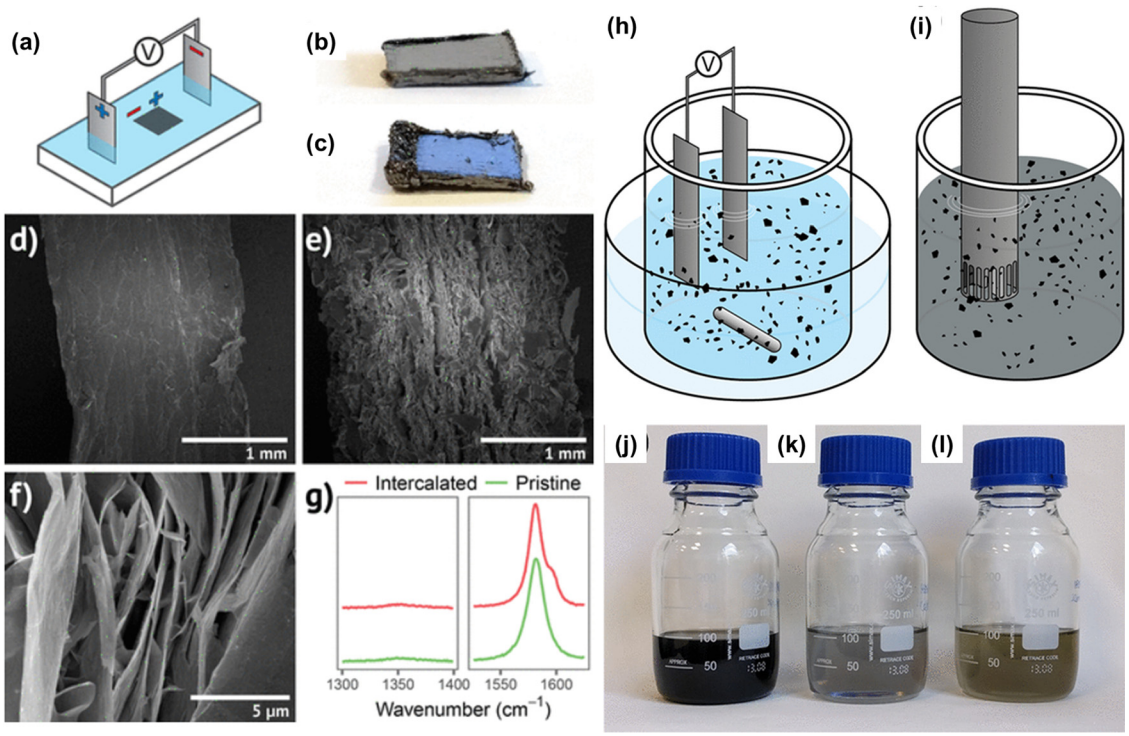

FIG. 8. (a) Schematic illustration of a bipolar electrochemical cell. Photographs of (b) pristine graphite foil and (c) Bu_4N^+ intercalated graphite foil. SEM images of the edges of (d) pristine graphite foil and (e,f) Bu_4N^+ intercalated graphite foil. (g) Raman spectra of the pristine and Bu_4N^+ intercalated graphite foil. Schematic illustration of the experimental setups for (h) high voltage bipolar electrochemistry and (i) subsequent high-shear exfoliation of intercalated graphite. Graphene dispersion in N-methyl-2-pyrrolidone (NMP) solvent from (j) both bipolar intercalation and high-shear exfoliation, (k) high-shear exfoliation with no electrochemical intercalation, and (l) combined bipolar electrochemistry and high-shear exfoliation without using Bu_4NBF_4 salt in the electrolyte. Reproduced with permission from Bjerglund *et al.*, ACS Omega **2**(10), 6492–6499 (2017). Copyright 2017 American Chemical Society.[168]

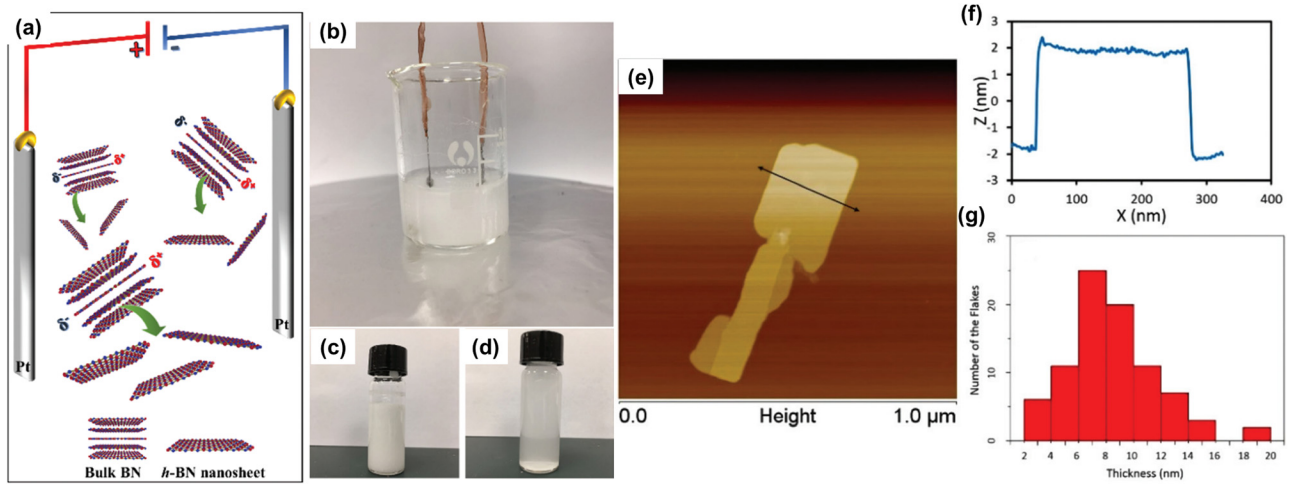

FIG. 9. (a) Schematic illustration and (b) photograph of bipolar electrochemical exfoliation of h-BN. (c) Pristine h-BN solution and (d) h-BN nanosheet obtained from bipolar electrochemical exfoliation. (e) AFM image of h-BN nanosheets obtained from bipolar exfoliation. (f) Corresponding height profiles of h-BN nanosheets from the black arrows in the AFM images. (g) Statistic analysis of the thickness distribution of exfoliated h-BN. Reproduced with permission from Wang *et al.*, Nanoscale **10**(15), 7298–7303 (2018). Copyright 2009 RSC Publishing.[172]

Na_2SO_4 had an average later size of 1.27 μm with a mean thickness of 8.4 nm [Figs. 8(e)–8(g)].[172] Although the size reduction mechanism of non-conductive material is not clearly understood, this work paved the way for the scalability of the electrochemical exfoliation system for not only the conducting materials, but also the layered insulators as well.[172]

III. APPLICATION AS ENERGY STORAGE DEVICES

The rapid growth of consumer electronics, electric vehicles, and grid integration of renewable energy sources has created enormous demand for energy storage devices that are safe, low cost, and capable of high power and energy output.[173] At the same time, efficient and green energy storage technologies are also critical to overcoming the environmental issues of fossil fuels as well as the availability of scarce natural resources used in batteries.[174] As electrochemical energy storage (EES) materials, 2D materials offer numerous advantageous features, including large active surface area, fast surface redox reactions, and shortened ion transport pathways. Existing literature has demonstrated that these properties can lead to improved charge storage capacity and rate capability of 2D materials in various EES systems, despite limitations posed by their restacking tendencies.[49,175] As an efficient method for synthesizing high-quality 2D materials, electrochemical exfoliation has been exploited to prepare electrodes for various alkali-metal ion batteries and supercapacitors.

A. Electrochemically exfoliated graphene-based electrodes

Electrochemically exfoliated graphene electrodes have been investigated as anode materials for metal-ion batteries due to their facile synthesis and low working potential.[64,176–179] For example, Jamaluddin *et al.* utilized electrochemically exfoliated graphene to encapsulate silicon (Si) nanoparticles and synthesized Si at graphene composites with a core-shell structure.[176] The Si at graphene composites was prepared via a spray-drying process using an aqueous suspension, in which a microsphere structure was formed *in situ* as graphene crumpled around Si nanoparticles [Fig. 10(a)].[176] This study revealed that the void space between graphene and Si can serve as a buffer to contain the volumetric expansion of Si nanoparticles within the core–shell structure, and the exfoliated graphene also provides high electrical conductivity and mechanical flexibility that improve rate performance and cycling stability.[176] In addition, the effect of graphene layers on the composite structure was investigated, and it was found that using graphene oxide or bi-layer and few-layered graphene as the shell material affected the electrical conductivity and capacity of the composite electrode.[176] As the best-performing combination, the Si at few-layered graphene (Si at FL-GB) anode delivered the highest initial discharge capacity up to 2882.3 mA h g^{-1} at 0.2 A g^{-1} as well as the highest initial Coulombic efficiency of 86.9% and excellent cycling stability of 1063.2 mA h g^{-1} at 0.5 A g^{-1} after 100 cycles with 70.9% capacity retention [Figs. 10(b)–10(d)].[176]

Wang *et al.* demonstrated vertically aligned MoS_2 nanosheets grown on electrochemically exfoliated graphene (EG) via solvothermal synthesis [Fig. 11(a)].[179] The vertically aligned structure on the graphene substrate increased the exposure of the active material and enhanced the charge transport kinetics through the vertical channels. The EG-MoS_2 anode delivered the capacities of 970 mA h g^{-1} at a high rate of 5 A g^{-1} and 1250 mA h g^{-1} after 100 cycles at 1 A g^{-1}. In a sodium-ion battery (SIB), the EG-MoS_2 anode also exhibited 509 mA h g^{-1} at 1 A g^{-1} after 250 cycles and 423 mA h g^{-1} at 2 A g^{-1} [Figs. 11(b)–11(d)].[179] Sun *et al.* also demonstrated a practical Li-ion full cell assembled with a $LiNi_{0.6}Co_{0.2}Mn_{0.2}O_2$ cathode and an exfoliated graphene (EG) anode, which was exfoliated in 0.1 M $(NH_4)_2SO_4$ aqueous solution at 10 V.[177] Due to the thin layers (~1.5 nm on average) and the high porosity of the exfoliated graphene sheets, the

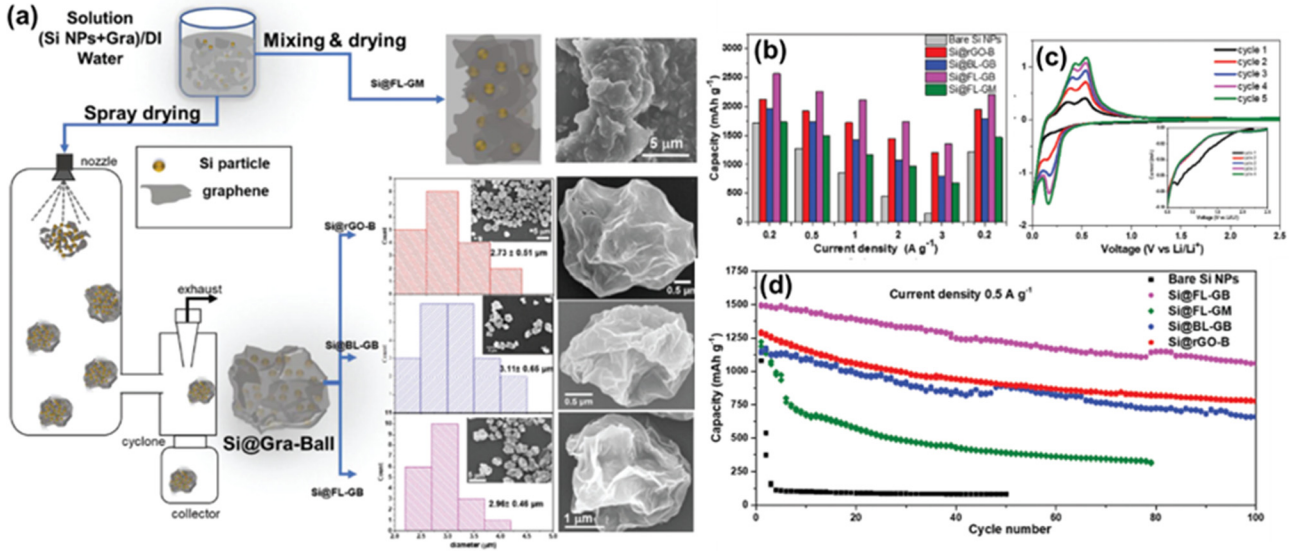

FIG. 10. (a) Schematic illustration for spray drying method for Si at Gra-balls preparation with SEM images and particle size distribution. (b) Electrochemical performance of Si nanoparticles and Si at Gra composites. (c) CV curves of Si at FL-GB at a scan rate of 0.1 mV s^{-1}. (d) Cycling stability of Si and Si at Gra composite electrodes at a current density of 0.5 A g^{-1}. Reproduced with permission from Jamaluddin *et al.*, Nanoscale **12**(17), 9616–9627 (2020). Copyright 2009 RSC Publishing.

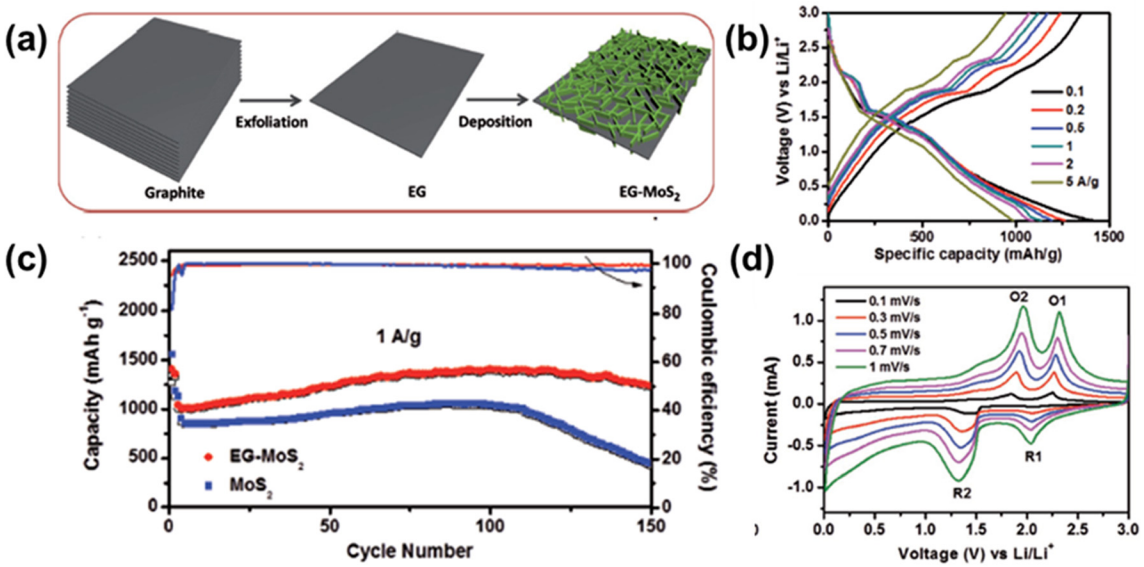

FIG. 11. (a) Schematic illustration of EG-MoS_2 preparation. The electrochemical performance curves. (b) Charge–discharge profiles of EG-MoS_2. (c) Cycling stability of EG-MoS_2 and MoS_2 at 1 A g^{-1}. (d) CV curves of EG-MoS_2 at different scan rates. Reproduced with permission from Wang *et al.*, Adv. Energy Mater. **8**(8), 1702254 (2018). Copyright 2017 John Wiley and Sons.

prelithiated EG anode delivered a reversible specific capacity of 360 mA h g^{-1} at 0.1 C and maintained a capacity of 206 mA h g^{-1} at a high current rate of 10 C.[177] At a low temperature of 0 °C, the EG anode still retained a capacity of ∼100 mA h g^{-1} at 5 C.[177] The full cell also exhibited a high energy density of ∼278 W h kg^{-1} and 100% capacity retention over 300 cycles.[177]

Similar approaches have also been explored for supercapacitor applications.[180–183] For example, Hamra *et al.* synthesized supercapacitor electrodes directly from electrochemically exfoliated graphene via vacuum filtration.[182] The graphene electrode was exfoliated using 1 M HNO_3 as an oxidizing agent, and 2 M KOH in polymer gel was used as an electrolyte. The supercapacitor delivered a specific capacitance of 2524.54 F g^{-1} at a current density of 0.5 A g^{-1} and retained >100% capacity after 1000 cycles.[182] Chih *et al.* also demonstrated an all-screen-printable method for fabricating all-solid and flexible microsupercapacitors (MSCs) with composite electrodes consisting of electrochemically exfoliated graphene and single-walled carbon nanotubes (CNTs).[181] In the hybrid electrode, CNTs serve as intermediates between graphene flakes to prevent restacking of graphene layers and promote ion transport. MSCs were prepared using a screen-printing process in which a pre-patterned screen was used to transfer the pattern to the underlying substrate, followed by electrolyte coating. As-synthesized flexible MSCs exhibited capacitances of 7.7 mF cm^{-2} and 77.3 F cm^{-3}, with >99% capacity retention after 15 000 cycles, and negligible capacitance loss with bending.[181]

Heteroatom-doped graphene electrodes such as nitrogen, boron, sulfur, and fluorine have also been studied by adjusting the electrolyte during exfoliation to achieve improved electrochemical performance.[83,111,180,184,185] For example, Jing and colleagues synthesized nitrogen-doped graphene (N-Gh) via alternating voltage electrochemical exfoliation at 5 V, where nitrogen doping was achieved with ammonium chloride and NaOH aqueous solution in the two-electrode system for exfoliation as shown in Fig. 12(a).[184] It was found that the nitrogen-doped graphene with 4.5% N atoms is much larger in size than the pristine graphene sheets and exhibits a more defective structure, probably due to the fast stripping and nitrogen-doping process.[184] In electrochemical tests, nitrogen doping also led to improvement in the specific capacitance and high-rate performance of N-Gh due to the additional pseudocapacitance from the nitrogen redox-active sites and the reduced restacking of graphene layers. The symmetrical N-Gh//N-Gh supercapacitor delivered an energy density of 4.76 W h kg^{-1} at a power density of 500 W kg^{-1} and retained 92.3% of its capacity after 5000 cycles [Figs. 12(b)–12(e)].[184] A similar effect achieved by fluorine doping of electrochemically exfoliated graphene was also investigated by Zhou *et al.*[111] Incorporation of fluorine has been shown to induce redox-active, semi-ionic C–F bonds, which also provide additional pseudocapacitance and improve charge storage performance as flexible microsupercapacitor electrodes. Muthu and Tatiparti also synthesized boron-incorporated reduced graphene oxide (B-rGO) via potentiostatic exfoliation using 0.1 M $(NH_4)_2SO_4$ + 0.5 M $B(OH)_3$ electrolyte.[185] Electron-deficient boron introduced a p-doping effect into B-rGO as shown by XPS, Raman and valence band spectra. The electrochemical performance of the B-rGO electrode was studied using 6 M KOH electrolyte in a three-electrode setup, where the rGO and B-rGO electrodes exhibited specific capacitances of 163 and 446 F g^{-1} at 0.1 A g^{-1}, and 111 and 284 F g^{-1} at 20 A g^{-1}, respectively.[185] B-rGO also showed excellent cycling stability with a capacity retention of 95.6% and a Coulombic efficiency of 97.4% after 2000 cycles.[185] The enhanced specific capacitance can be attributed to the p-doping effect of boron in B-rGO, which can accommodate more charge storage.

B. Other 2D atomic layer material-based electrodes

In addition to graphene, other 2D atomic layer materials produced by electrochemical exfoliation have also been successfully

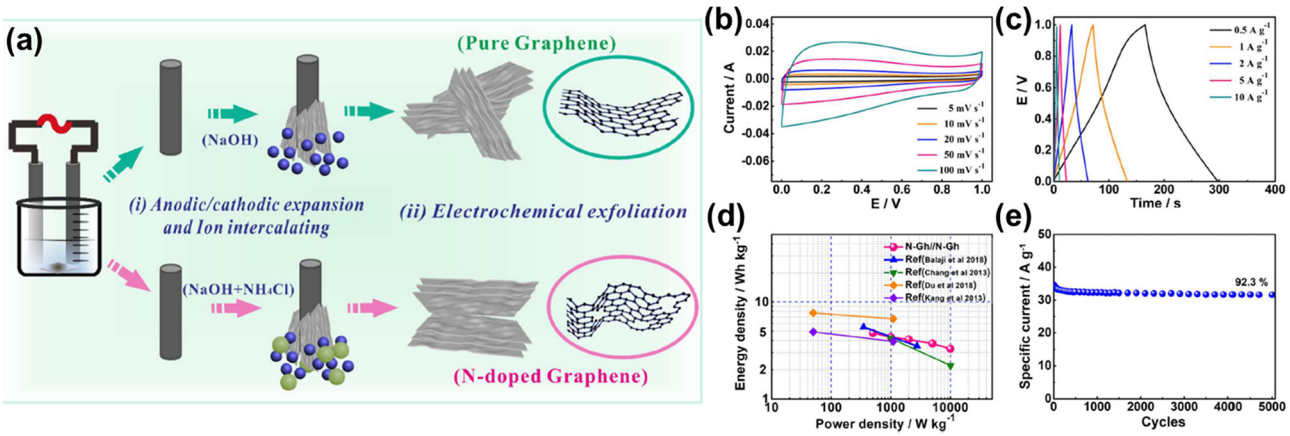

FIG. 12. (a) Schematic illustration of the electrochemical exfoliation of pure graphene and nitrogen-doped graphene (N-Gh) samples. The electrochemical performance curves of N-Gh. (b) The CV profiles of N-Gh at various scan rates. (d) Galvanostatic charge–discharge profiles of N-Gh//N-Gh with varying current densities. (d) Ragone plots of N-Gh/N-Gh. (e) Cycling stability of N-Gh//N-Gh at a current density of 0.5 A g^{-1}. Reproduced with permission from Jing *et al.*, Front. Chem. **8**, 428 (2020). Copyright 2020 Authors, licensed under a Creative Commons Attribution (CC BY) License.[184]

incorporated into energy storage devices.[67,146,156,186–189] For example, the cathodic exfoliation of bulk antimony (Sb) to porous antimonene was investigated by Yang and co-workers.[190] The exfoliation process was carried out in a two-electrode cell under a voltage of −5 V in 1 M tetramethylammonium hydroxide (TMAOH) aqueous solution.[190] This study suggests that Sb exfoliated in an alkaline solution is more stable than using organic electrolytes and Na_2SO_4, which leads to the formation of aggregated nanoparticles.[190] As an anode material in SIBs, the antimonene electrode delivered a high specific capacity of 569.1 mA h g^{-1} upon 200 cycles at 0.1 A g^{-1} and maintained 277.8 mA h g^{-1} at 5 A g^{-1}.[190] Huang *et al.* also utilized electrochemical cationic intercalation to prepare large few-layered phosphorene flakes without surface functional groups.[156] The authors successfully controlled the phosphorene thickness between 2 and 11 layers by adjusting the intercalation rate of the tetraalkylammonium cations with different applied potentials (−5–−15 V).[156] The phosphorene anode in SIBs delivered a high capacity of 1968 mA h g^{-1} at a current density of 100 mA g^{-1} and retained 603.3 mA h g^{-1} after 100 cycles at 1.5 A g^{-1}.[156] Ultrasonication-assisted electrochemical exfoliation of few-layered bismuthene nanosheets (FBNs) was investigated by Shen and colleagues.[191] As shown in Fig. 13(a), the intercalation reaction was performed in a sonication bath using a two-electrode setup consisting of a bismuth crystal working electrode and a platinum counter electrode for 8 h.[191] Owing to the exfoliated 2D architecture, the exfoliated FBNs possess a larger active surface area, improved K-ion kinetics, and higher structural stability against volume changes during the potassiation/depotassiation process [Fig. 13(c)].[191] The FBN anode in a potassium ion battery (KIB) exhibited a charge−discharge capacity of 423 mA h g^{-1} at a current density of 2.5 A g^{-1} and impressive cycling stability by maintaining 201 mA h g^{-1} at 20 A g^{-1} over 2500 cycles [Figs. 13(b) and 13(d)].[191]

Li *et al.* presented a novel anodic and cathodic simultaneous exfoliation method for synthesizing composite 2D materials.[187] This method combines anodic exfoliation of graphene and cathodic exfoliation of other 2D materials including MoS_2, MnO_2, and graphitic carbon nitride (g-C_3N_4) in a one-pot setup [Figs. 14(a)–14(c)].[187] Notably, the incorporation of conductive additives into the electrodes was demonstrated to enable the exfoliation of 2D nanomaterials regardless of the conductivity of the bulk precursor.[187] Among the various combinations, the MnO_2 and graphene composite (MnO_2-G) was tested in symmetrical all-solid-state supercapacitors using a polyvinyl alcohol/H_3PO_4 gel electrolyte.[187] The supercapacitor delivered the specific capacitances of 265 F g^{-1} at 2.5 A g^{-1} and 212 F g^{-1} at 50 A g^{-1} with capacitance retention of 94% over 5000 cycles, comparable to other state-of-the-art devices based on MnO_2–carbon composites [Figs. 14(d) and 14(e)].[187] MoS_2–graphene and g-C_3N_4–graphene composite films were also demonstrated to be effective hydrogen evolution catalysts.[187] Hu *et al.* also studied the electrochemically exfoliated MoS_2 electrode in supercapacitors.[186] MoS_2 powder fixed with carbon cloth was exfoliated in a 0.5 M Na_2SO_4 solution at 10 V to obtain 1–3 μm MoS_2 nanosheets with an average thickness of 3 nm (~4 layers).[186] In a three-electrode test system with 0.5 M KOH electrolyte, MoS_2 nanosheets showed superior performance compared to bulk MoS_2, delivering 285 F g^{-1} at 2 A g^{-1} and 83.8% capacitance retention after 500 cycles.[186] Finally, Yang *et al.* obtained few-layered BP nanoflakes from bulk BP crystals by applying +10 V in 0.5 M Na_2SO_4 aqueous solution.[119] The free-standing BP films exhibited an energy density of 3.63 mW h cm^{-3}, a power density of 10.1 W cm^{-3}, and a capacity retention of 94.3% after 50 000 cycles at a current density of 0.2 A cm^{-3}.[119]

IV. CONCLUSIONS AND FUTURE OUTLOOK

Electrochemical exfoliation techniques are gaining momentum with the increasing demand for 2D atomic layer materials with superior electrochemical properties and the growing importance of their industrial-level scalability. This review has comprehensively summarized recent research advances in the electrochemical exfoliation of 2D materials, including four different techniques and their unique characteristics, as well as the applications of exfoliated 2D materials for various energy storage devices. A high percentage of few-layered atomically thin 2D materials with relatively large sizes can be obtained via the aqueous-phase anodic exfoliation process. Cathodic exfoliation

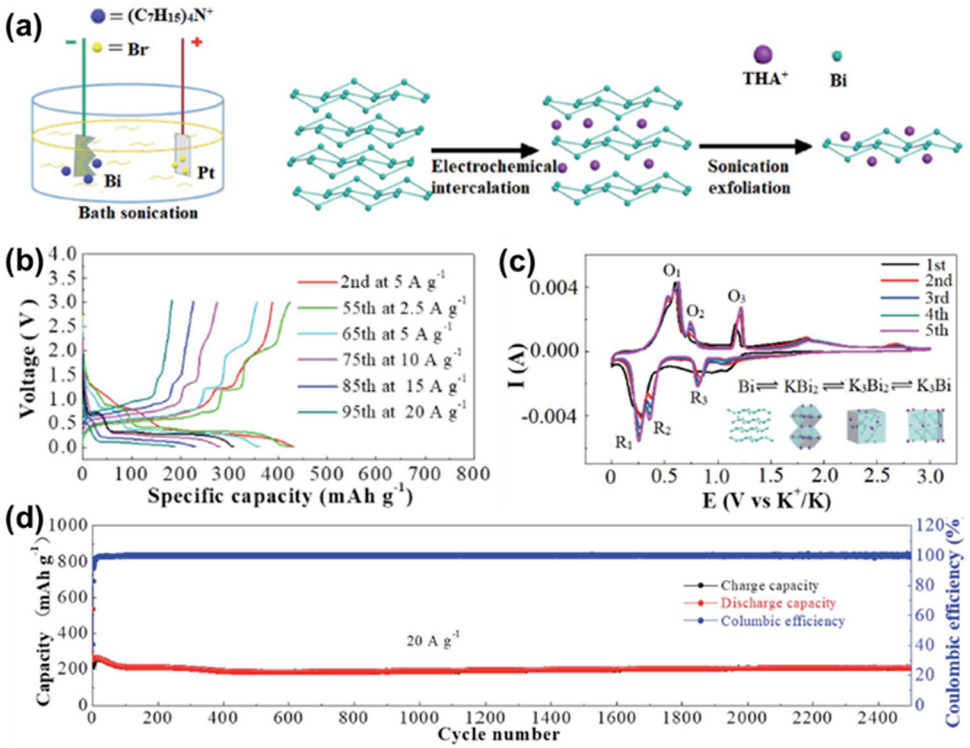

FIG. 13. (a) Schematic illustration of electrochemical exfoliation for FBN production. (b) Galvanostatic charge and discharge curves of FBNs at various current densities. (c) Cyclic voltammetry of FBNs at a scan rate of 0.1 mV s^{-1} with the illustration of potassiation−depotassiation processes. (d) Cycling performance for 2500 cycles. Reproduced from Shen *et al.*, J. Mater. Chem. A **8**(1), 453–460 (2020). Copyright 2020 RSC publishing.

offers a promising route to fabricate 2D materials with negligible oxidation and high crystallinity. Dual exfoliation combines both anodic and cathodic exfoliation processes simultaneously, allowing fast and efficient exfoliation of 2D materials. Finally, the bipolar method allows the exfoliation of layered materials in various forms such as foils, rods, and even powders. The bipolar configuration allows the exfoliation of semiconducting 2D materials and electrical insulators (i.e., h-BN and TMDs), but with long reaction times and low exfoliation yield.

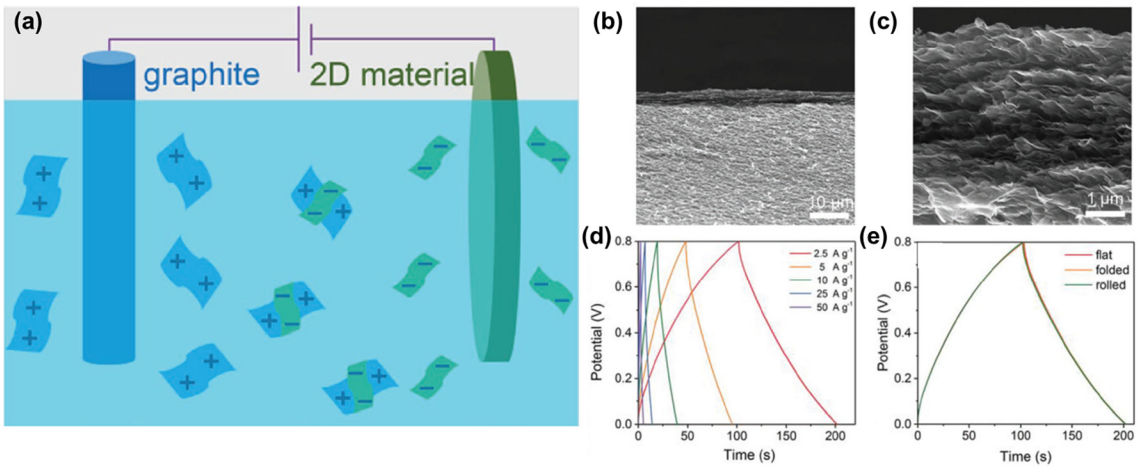

FIG. 14. (a) Schematic illustration of simultaneous electrochemical exfoliation. [(b) and (c)] SEM images of cross-sectional MnO_2-G film. Galvanostatic charge–discharge curves of the planar, symmetric all-solid-state supercapacitor device (d) at different current densities and (e) at a current density of 2.5 A g^{-1} at different mechanical conditions. Reproduced from Li *et al.*, Adv. Energy Mater. **8**(12), 1702794 (2018). Copyright 2018 John Wiley and Sons.

An ideal electrochemical exfoliation method would be to fabricate 2D materials in a highly controllable manner, allowing the fabrication of materials with structural and property tuning for specific target applications. Therefore, the main challenge in the exfoliation process is to precisely control the structures of the exfoliated products such as the number of layers, size, oxidation, and defects, as well as solvent residues and contamination. In addition, recent studies have shown that specific functional groups can be incorporated into exfoliated 2D material during the electrochemical process, providing another opportunity to tailor the structure and properties of 2D materials.[80,81,192,193] A fundamental understanding of the electrochemical exfoliation mechanisms can contribute to improving the production efficiency of 2D materials and controlling their structures and properties. The electrochemical exfoliation process of 2D layered materials is a collective phenomenon consisting of several reactions, including ion intercalation, gas evolution, interlayer expansion, and irreversible exfoliation. These reactions do not necessarily occur sequentially and occur non-uniformly within the material, resulting in non-uniform exfoliation products. However, a comprehensive understanding of the mechanical details of each reaction and the role of each reaction in controlling the structure of 2D materials are still lacking. Given interconnected multiple reactions in the electrochemical process, computer simulation and *operando* (or *in situ*) monitoring of the process are extremely helpful in understanding the complex exfoliation mechanisms. For example, *in situ* AFM studies of graphite during ion intercalation successfully demonstrated potential-dependent interlayer expansion due to ion intercalation and gas evolution.[194,195] Another study using *in situ* optical and Raman spectroscopy suggested that the two characteristic stages, nondestructive intercalation and subsequent gas evolution, are key steps in an efficient exfoliation process.[196] Moreover, a recent study has correlated the exfoliation efficiency of graphene in the anodic exfoliation system with the binding energy of electrolyte anions on graphene.[102] Understanding and predicting phenomena through computer simulation is a step forward from optimizing parameters through iterative experiments and is expected to accelerate the development of electrochemical stripping processes.

Electrochemical exfoliation techniques often require post-treatment to further reduce the number of layers and stably disperse the 2D materials. However, prolonged post-treatment processes such as sonication and delithiation can compromise the quality of the final product. Therefore, direct electrochemical exfoliation of bulk layered crystals into single or few 2D materials without post-treatment is highly required to improve overall manufacturing efficiency and cost. In addition, conventional electrochemical exfoliation processes mainly rely on large bulk crystals and large amounts of electrolytes, which are expensive for large-scale industrial applications. Therefore, there is an urgent need to develop new electrochemical setups that can utilize low-cost power and small amounts of electrolyte to minimize the manufacturing cost of 2D materials. In summary, understanding the mechanical details of the electrochemical exfoliation mechanism and realizing the electrochemical setup for producing cost-effective, structure-controlled 2D material are critical for the commercialization of 2D materials in a variety of electrochemical applications, including catalysis, electrochemical sensors, and energy storage devices.

ACKNOWLEDGMENTS

This material is based upon work supported by the National Science Foundation under Grant No. 1751693.

AUTHOR DECLARATIONS

Conflict of Interest

The authors have no conflicts to disclose.

Author Contributions

Hoyoung Lee: Conceptualization (equal); Funding acquisition (lead); Investigation (equal); Project administration (lead); Supervision (lead); Writing – original draft (equal); Writing – review & editing (equal). **Shikai Jin:** Conceptualization (equal); Investigation (equal); Writing – original draft (equal); Writing – review & editing (equal). **Jiyong Chung:** Investigation (equal); Writing – original draft (equal); Writing – review & editing (equal). **Minsu Kim:** Investigation (supporting); Writing – original draft (supporting); Writing – review & editing (equal). **Seung Woo Lee:** Conceptualization (equal); Funding acquisition (lead); Investigation (supporting); Project administration (lead); Supervision (lead); Writing – original draft (equal); Writing – review & editing (equal).

DATA AVAILABILITY

Data sharing is not applicable to this article as no new data were created or analyzed in this study.

REFERENCES

[1]K. S. Novoselov *et al.*, "Electric field effect in atomically thin carbon films," Science **306**(5696), 666–669 (2004).
[2]D. G. Papageorgiou, I. A. Kinloch, and R. J. Young, "Mechanical properties of graphene and graphene-based nanocomposites," Prog. Mater. Sci. **90**, 75–127 (2017).
[3]A. A. Balandin, "Thermal properties of graphene and nanostructured carbon materials," Nat. Mater. **10**(8), 569–581 (2011).
[4]T. V. Cuong *et al.*, "Optoelectronic properties of graphene thin films prepared by thermal reduction of graphene oxide," Mater. Lett. **64**(6), 765–767 (2010).
[5]M.-S. Cao, X.-X. Wang, W.-Q. Cao, and J. Yuan, "Ultrathin graphene: Electrical properties and highly efficient electromagnetic interference shielding," J. Mater. Chem. C **3**(26), 6589–6599 (2015).
[6]X. Ling, H. Wang, S. Huang, F. Xia, and M. S. Dresselhaus, "The renaissance of black phosphorus," Proc. Natl. Acad. Sci. **112**(15), 4523–4530 (2015).
[7]S. Manzeli, D. Ovchinnikov, D. Pasquier, O. V. Yazyev, and A. Kis, "2D transition metal dichalcogenides," Nat. Rev. Mater. **2**(8), 17033 (2017).
[8]B. Anasori, M. R. Lukatskaya, and Y. Gogotsi, "2D metal carbides and nitrides (MXenes) for energy storage," Nat. Rev. Mater. **2**(2), 16098 (2017).
[9]K. Zhang, Y. Feng, F. Wang, Z. Yang, and J. Wang, "Two dimensional hexagonal boron nitride (2D-hBN): Synthesis, properties and applications," J. Mater. Chem. C **5**(46), 11992–12022 (2017).
[10]J. W. Colson *et al.*, "Oriented 2D covalent organic framework thin films on single-layer graphene," Science **332**(6026), 228–231 (2011).
[11]J. R. Schaibley *et al.*, "Valleytronics in 2D materials," Nat. Rev. Mater. **1**(11), 16055 (2016).
[12]R. Mas-Ballesté, C. Gómez-Navarro, J. Gómez-Herrero, and F. Zamora, "2D materials: To graphene and beyond," Nanoscale **3**(1), 20–30 (2011).
[13]A. Gupta, T. Sakthivel, and S. Seal, "Recent development in 2D materials beyond graphene," Prog. Mater. Sci. **73**, 44–126 (2015).
[14]K. S. Novoselov, A. Mishchenko, A. Carvalho, and A. H. Castro Neto, "2D materials and van der Waals heterostructures," Science **353**(6298), aac9439 (2016).

[15]D. S. Schulman, A. J. Arnold, and S. Das, "Contact engineering for 2D materials and devices," Chem. Soc. Rev. **47**(9), 3037–3058 (2018).
[16]K. Chen, S. Song, F. Liu, and D. Xue, "Structural design of graphene for use in electrochemical energy storage devices," Chem. Soc. Rev. **44**(17), 6230–6257 (2015).
[17]R. Raccichini, A. Varzi, S. Passerini, and B. Scrosati, "The role of graphene for electrochemical energy storage," Nat. Mater. **14**(3), 271–279 (2015).
[18]A. F. Khan, D. A. C. Brownson, E. P. Randviir, G. C. Smith, and C. E. Banks, "2D hexagonal boron nitride (2D-hBN) explored for the electrochemical sensing of dopamine," Anal. Chem. **88**(19), 9729–9737 (2016).
[19]H. Ilatikhameneh, Y. Tan, B. Novakovic, G. Klimeck, R. Rahman, and J. Appenzeller, "Tunnel field-effect transistors in 2-D transition metal dichalcogenide materials," IEEE J. Explor. Solid-State Comput. Devices Circuits **1**, 12–18 (2015).
[20]B. Mendoza-Sánchez and Y. Gogotsi, "Synthesis of two-dimensional materials for capacitive energy storage," Adv. Mater. **28**(29), 6104–6135 (2016).
[21]B. Deng, Z. Liu, and H. Peng, "Toward mass production of CVD graphene films," Adv. Mater. **31**(9), 1800996 (2019).
[22]C. Backes *et al.*, "Production and processing of graphene and related materials," 2D Mater. **7**(2), 022001 (2020).
[23]W. A. de Heer *et al.*, "Epitaxial graphene," Solid State Commun. **143**(1), 92–100 (2007).
[24]P. W. Sutter, J.-I. Flege, and E. A. Sutter, "Epitaxial graphene on ruthenium," Nat. Mater. **7**(5), 406–411 (2008).
[25]L. Gao, J. R. Guest, and N. P. Guisinger, "Epitaxial graphene on Cu(111)," Nano Lett. **10**(9), 3512–3516 (2010).
[26]G. Li *et al.*, "Epitaxial growth and physical properties of 2D materials beyond graphene: From monatomic materials to binary compounds," Chem. Soc. Rev. **47**(16), 6073–6100 (2018).
[27]J. L. Zhang *et al.*, "2D phosphorene: Epitaxial growth and interface engineering for electronic devices," Adv. Mater. **30**(47), 1802207 (2018).
[28]L. Zhang, P. Peng, and F. Ding, "Epitaxial growth of 2D materials on high-index substrate surfaces," Adv. Funct. Mater. **31**(29), 2100503 (2021).
[29]M. Choucair, P. Thordarson, and J. A. Stride, "Gram-scale production of graphene based on solvothermal synthesis and sonication," Nat. Nanotechnol. **4**(1), 30–33 (2009).
[30]A. V. Murugan, T. Muraliganth, and A. Manthiram, "Rapid, facile microwave-solvothermal synthesis of graphene nanosheets and their polyaniline nanocomposites for energy storage," Chem. Mater. **21**(21), 5004–5006 (2009).
[31]D. Deng *et al.*, "Toward N-doped graphene via solvothermal synthesis," Chem. Mater. **23**(5), 1188–1193 (2011).
[32]L. Chen, Y. Hernandez, X. Feng, and K. Müllen, "From nanographene and graphene nanoribbons to graphene sheets: Chemical synthesis," Angew. Chem. Int. Ed. **51**(31), 7640–7654 (2012).
[33]S. Eigler *et al.*, "Wet chemical synthesis of graphene," Adv. Mater. **25**(26), 3583–3587 (2013).
[34]G. Huang *et al.*, "Graphene-like MoS_2/graphene composites: Cationic surfactant-assisted hydrothermal synthesis and electrochemical reversible storage of lithium," Small **9**(21), 3693–3703 (2013).
[35]C. Berger *et al.*, "Ultrathin epitaxial graphite: 2D electron gas properties and a route toward graphene-based nanoelectronics," J. Phys. Chem. B **108**(52), 19912–19916 (2004).
[36]E. Loginova, N. C. Bartelt, P. J. Feibelman, and K. F. McCarty, "Evidence for graphene growth by C cluster attachment," New J. Phys. **10**(9), 093026 (2008).
[37]E. Moreau *et al.*, "Graphene growth by molecular beam epitaxy on the carbon-face of SiC," Appl. Phys. Lett. **97**(24), 241907 (2010).
[38]C.-L. Song *et al.*, "Molecular-beam epitaxy and robust superconductivity of stoichiometric FeSe crystalline films on bilayer graphene," Phys. Rev. B **84**(2), 020503 (2011).
[39]J. M. Garcia *et al.*, "Graphene growth on h-BN by molecular beam epitaxy," Solid State Commun. **152**(12), 975–978 (2012).
[40]K. S. Kim *et al.*, "Large-scale pattern growth of graphene films for stretchable transparent electrodes," Nature **457**(7230), 706–710 (2009).
[41]Y. Zhang, L. Zhang, and C. Zhou, "Review of chemical vapor deposition of graphene and related applications," Acc. Chem. Res. **46**(10), 2329–2339 (2013).
[42]H. F. Liu, S. L. Wong, and D. Z. Chi, "CVD growth of MoS_2-based two-dimensional materials," Chem. Vap. Deposition **21**(10–12), 241–259 (2015).
[43]X. Li, L. Colombo, and R. S. Ruoff, "Synthesis of graphene films on copper foils by chemical vapor deposition," Adv. Mater. **28**(29), 6247–6252 (2016).
[44]S. M. Kim *et al.*, "Synthesis of large-area multilayer hexagonal boron nitride for high material performance," Nat. Commun. **6**(1), 8662 (2015).
[45]H. Yu *et al.*, "Wafer-scale growth and transfer of highly-oriented monolayer MoS_2 continuous films," ACS Nano **11**(12), 12001–12007 (2017).
[46]J. Shim *et al.*, "Controlled crack propagation for atomic precision handling of wafer-scale two-dimensional materials," Science **362**(6415), 665–670 (2018).
[47]Z. Gao *et al.*, "Large-area epitaxial growth of curvature-stabilized ABC trilayer graphene," Nat. Commun. **11**(1), 546 (2020).
[48]M. Wang *et al.*, "Single-crystal, large-area, fold-free monolayer graphene," Nature **596**(7873), 519–524 (2021).
[49]X. Zhang, L. Hou, A. Ciesielski, and P. Samorì, "2D materials beyond graphene for high-performance energy storage applications," Adv. Energy Mater. **6**(23), 1600671 (2016).
[50]W. S. Hummers, Jr. and R. E. Offeman, "Preparation of graphitic oxide," J. Am. Chem. Soc. **80**(6), 1339–1339 (1958).
[51]G. Eda, H. Yamaguchi, D. Voiry, T. Fujita, M. Chen, and M. Chhowalla, "Photoluminescence from chemically exfoliated MoS_2," Nano Lett. **11**(12), 5111–5116 (2011).
[52]M. Yi and Z. Shen, "A review on mechanical exfoliation for the scalable production of graphene," J. Mater. Chem. A **3**(22), 11700–11715 (2015).
[53]J. N. Coleman *et al.*, "Two-dimensional nanosheets produced by liquid exfoliation of layered materials," Science **331**(6017), 568–571 (2011).
[54]Y. Hernandez *et al.*, "High-yield production of graphene by liquid-phase exfoliation of graphite," Nat. Nanotechnol. **3**(9), 563–568 (2008).
[55]K. R. Paton *et al.*, "Scalable production of large quantities of defect-free few-layer graphene by shear exfoliation in liquids," Nat. Mater. **13**(6), 624–630 (2014).
[56]E. Varrla *et al.*, "Turbulence-assisted shear exfoliation of graphene using household detergent and a kitchen blender," Nanoscale **6**(20), 11810–11819 (2014).
[57]G. Guan *et al.*, "Protein induces layer-by-layer exfoliation of transition metal dichalcogenides," J. Am. Chem. Soc. **137**(19), 6152–6155 (2015).
[58]J. Lu, J.-X. Yang, J. Wang, A. Lim, S. Wang, and K. P. Loh, "One-pot synthesis of fluorescent carbon nanoribbons, nanoparticles, and graphene by the exfoliation of graphite in ionic liquids," ACS Nano **3**(8), 2367–2375 (2009).
[59]J. Wang, K. K. Manga, Q. Bao, and K. P. Loh, "High-yield synthesis of few-layer graphene flakes through electrochemical expansion of graphite in propylene carbonate electrolyte," J. Am. Chem. Soc. **133**(23), 8888–8891 (2011).
[60]J. Huang *et al.*, "Electrochemical exfoliation of pillared-layer metal–organic framework to boost the oxygen evolution reaction," Angew. Chem. Int. Ed. **57**(17), 4632–4636 (2018).
[61]J. Lee, S. Noh, N. D. Pham, and J. H. Shim, "Top-down synthesis of S-doped graphene nanosheets by electrochemical exfoliation of graphite: Metal-free bifunctional catalysts for oxygen reduction and evolution reactions," Electrochim. Acta **313**, 1–9 (2019).
[62]Y. Zhang, X. Zhang, Y. Ling, F. Li, A. M. Bond, and J. Zhang, "Controllable synthesis of few-layer bismuth subcarbonate by electrochemical exfoliation for enhanced CO_2 reduction performance," Angew. Chem. Int. Ed. **57**(40), 13283–13287 (2018).
[63]S. X. Leong, C. C. Mayorga-Martinez, X. Chia, J. Luxa, Z. Sofer, and M. Pumera, "2H → 1T phase change in direct synthesis of WS_2 nanosheets via solution-based electrochemical exfoliation and their catalytic properties," ACS Appl. Mater. Interfaces **9**(31), 26350–26356 (2017).
[64]X. Zhao *et al.*, "Electrochemical exfoliation of graphene as an anode material for ultra-long cycle lithium ion batteries," J. Phys. Chem. Solids **139**, 109301 (2020).
[65]Y. Munaiah, P. Ragupathy, and V. K. Pillai, "Single-step synthesis of halogenated graphene through electrochemical exfoliation and its utilization as electrodes for zinc bromine redox flow battery," J. Electrochem. Soc. **163**(14), A2899–A2910 (2016).
[66]H. Shuai *et al.*, "Electrochemically exfoliated phosphorene–graphene hybrid for sodium-ion batteries," Small Methods **3**(2), 1800328 (2019).
[67]Y. Yang *et al.*, "Controllable fabrication of two-dimensional layered transition metal oxides through electrochemical exfoliation of non-van der Waals metals for rechargeable zinc-ion batteries," Chem. Eng. J. **408**, 127247 (2021).

[68]A. Jamaluddin *et al.*, "Fluorinated graphene as a dual-functional anode to achieve dendrite-free and high-performance lithium metal batteries," Carbon **197**, 141–151 (2022).
[69]A. Ejigu *et al.*, "On the role of transition metal salts during electrochemical exfoliation of graphite: Antioxidants or metal oxide decorators for energy storage applications," Adv. Funct. Mater. **28**(48), 1804357 (2018).
[70]Z. Liu, Z.-S. Wu, S. Yang, R. Dong, X. Feng, and K. Müllen, "Ultraflexible in-plane micro-supercapacitors by direct printing of solution-processable electrochemically exfoliated graphene," Adv. Mater. **28**(11), 2217–2222 (2016).
[71]Z. Dou, Z. Qin, Y. Shen, S. Hu, N. Liu, and Y. Zhang, "High-performance flexible supercapacitor based on carbon cloth through in-situ electrochemical exfoliation and re-deposition in neutral electrolyte," Carbon **153**, 617–624 (2019).
[72]P. Das, L. Zhang, S. Zheng, X. Shi, Y. Li, and Z.-S. Wu, "Rapid fabrication of high-quality few-layer graphene through gel-phase electrochemical exfoliation of graphite for high-energy-density ionogel-based micro-supercapacitors," Carbon **196**, 203–212 (2022).
[73]M. B. Erande, M. S. Pawar, and D. J. Late, "Humidity sensing and photodetection behavior of electrochemically exfoliated atomically thin-layered black phosphorus nanosheets," ACS Appl. Mater. Interfaces **8**(18), 11548–11556 (2016).
[74]G. Maccaferri *et al.*, "Highly sensitive amperometric sensor for morphine detection based on electrochemically exfoliated graphene oxide. Application in screening tests of urine samples," Sens. Actuators, B **281**, 739–745 (2019).
[75]J. Li *et al.*, "Electrochemical exfoliation of naturally occurring layered mineral stibnite (Sb_2S_3) for highly sensitive and fast room-temperature acetone sensing," Adv. Mater. Interfaces **9**(19), 2200605 (2022).
[76]P. Shukla, P. Saxena, D. Madhwal, N. Bhardwaj, and V. K. Jain, "Battery-operated resistive sensor based on electrochemically exfoliated pencil graphite core for room temperature detection of LPG," Sens. Actuators, B **343**, 130133 (2021).
[77]M. U. Arshad *et al.*, "Multi-functionalized fluorinated graphene composite coating for achieving durable electronics: Ultralow corrosion rate and high electrical insulating passivation," Carbon **195**, 141–153 (2022).
[78]K. Parvez *et al.*, "Electrochemically exfoliated graphene as solution-processable, highly conductive electrodes for organic electronics," ACS Nano **7**(4), 3598–3606 (2013).
[79]Y. Kim, Y. J. Kwon, J.-Y. Hong, M. Park, C. J. Lee, and J. U. Lee, "Spray coating of electrochemically exfoliated graphene/conducting polymer hybrid electrode for organic field effect transistor," J. Ind. Eng. Chem. **68**, 399–405 (2018).
[80]A. Ejigu, I. A. Kinloch, and R. A. W. Dryfe, "Single stage simultaneous electrochemical exfoliation and functionalization of graphene," ACS Appl. Mater. Interfaces **9**(1), 710–721 (2017).
[81]Y. Zhuo, I. A. Kinloch, and M. A. Bissett, "Simultaneous electrochemical exfoliation and chemical functionalization of graphene for supercapacitor electrodes," J. Electrochem. Soc. **167**(11), 110531 (2020).
[82]S. Fang, Y. Lin, and Y. H. Hu, "Recent advances in green, safe, and fast production of graphene oxide via electrochemical approaches," ACS Sustainable Chem. Eng. **7**(15), 12671–12681 (2019).
[83]N. Parveen, M. O. Ansari, S. A. Ansari, and M. H. Cho, "Simultaneous sulfur doping and exfoliation of graphene from graphite using an electrochemical method for supercapacitor electrode materials," J. Mater. Chem. A **4**(1), 233–240 (2016).
[84]X. Lu and C. Zhao, "Controlled electrochemical intercalation, exfoliation and in situ nitrogen doping of graphite in nitrate-based protic ionic liquids," Phys. Chem. Chem. Phys. **15**(46), 20005–20009 (2013).
[85]V. Thirumal *et al.*, "Single pot electrochemical synthesis of functionalized and phosphorus doped graphene nanosheets for supercapacitor applications," J. Mater. Sci.: Mater. Electron. **26**(8), 6319–6328 (2015).
[86]P. Shi *et al.*, "Simultaneously exfoliated boron-doped graphene sheets to encapsulate sulfur for applications in lithium–sulfur batteries," ACS Sustainable Chem. Eng. **6**(8), 9661–9670 (2018).
[87]A. Ejigu, B. Miller, I. A. Kinloch, and R. A. W. Dryfe, "Optimisation of electrolytic solvents for simultaneous electrochemical exfoliation and functionalisation of graphene with metal nanostructures," Carbon **128**, 257–266 (2018).
[88]W. Wu, C. Zhang, and S. Hou, "Electrochemical exfoliation of graphene and graphene-analogous 2D nanosheets," J. Mater. Sci. **52**(18), 10649–10660 (2017).
[89]Y. Fang *et al.*, "Janus electrochemical exfoliation of two-dimensional materials," J. Mater. Chem. A **7**(45), 25691–25711 (2019).
[90]Y. Zhang and Y. Xu, "Simultaneous electrochemical dual-electrode exfoliation of graphite toward scalable production of high-quality graphene," Adv. Funct. Mater. **29**(37), 1902171 (2019).
[91]M. H. Dalal, C.-Y. Lee, and G. G. Wallace, "Simultaneous anodic and cathodic exfoliation of graphite electrodes in an aqueous solution of inorganic salt," ChemElectroChem **8**(16), 3168–3173 (2021).
[92]H. Hashimoto, Y. Muramatsu, Y. Nishina, and H. Asoh, "Bipolar anodic electrochemical exfoliation of graphite powders," Electrochem. Commun. **104**, 106475 (2019).
[93]S. M. Tan, C. C. Mayorga-Martinez, Z. Sofer, and M. Pumera, "Bipolar electrochemistry exfoliation of layered metal chalcogenides Sb_2S_3 and Bi_2S_3 and their hydrogen evolution applications," Chem. Eur. J. **26**(29), 6479–6483 (2020).
[94]A. Rabiei Baboukani, I. Khakpour, V. Drozd, A. Allagui, and C. Wang, "Single-step exfoliation of black phosphorus and deposition of phosphorene via bipolar electrochemistry for capacitive energy storage application," J. Mater. Chem. A **7**(44), 25548–25556 (2019).
[95]G. Wang, B. Wang, J. Park, Y. Wang, B. Sun, and J. Yao, "Highly efficient and large-scale synthesis of graphene by electrolytic exfoliation," Carbon **47**(14), 3242–3246 (2009).
[96]C.-Y. Su, A.-Y. Lu, Y. Xu, F.-R. Chen, A. N. Khlobystov, and L.-J. Li, "High-quality thin graphene films from fast electrochemical exfoliation," ACS Nano **5**(3), 2332–2339 (2011).
[97]F. Kang, Y. Leng, and T.-Y. Zhang, "Influences of H_2O_2 on synthesis of H_2SO_4-GICs," J. Phys. Chem. Solids **57**(6), 889–892 (1996).
[98]K. Parvez *et al.*, "Exfoliation of graphite into graphene in aqueous solutions of inorganic salts," J. Am. Chem. Soc. **136**(16), 6083–6091 (2014).
[99]F. Beck, J. Jiang, and H. Krohn, "Potential oscillations during galvanostatic overoxidation of graphite in aqueous sulphuric acids," J. Electroanal. Chem. **389**(1), 161–165 (1995).
[100]F. Beck, H. Junge, and H. Krohn, "Graphite intercalation compounds as positive electrodes in galvanic cells," Electrochim. Acta **26**(7), 799–809 (1981).
[101]C. A. Goss, J. C. Brumfield, E. A. Irene, and R. W. Murray, "Imaging the incipient electrochemical oxidation of highly oriented pyrolytic-graphite," Anal. Chem. **65**(10), 1378–1389 (1993) (in English).
[102]H. Lee, J. I. Choi, J. Park, S. S. Jang, and S. W. Lee, "Role of anions on electrochemical exfoliation of graphite into graphene in aqueous acids," Carbon **167**, 816–825 (2020).
[103]S. Yang *et al.*, "Organic radical-assisted electrochemical exfoliation for the scalable production of high-quality graphene," J. Am. Chem. Soc. **137**(43), 13927–13932 (2015).
[104]C.-H. Chen, S.-W. Yang, M.-C. Chuang, W.-Y. Woon, and C.-Y. Su, "Towards the continuous production of high crystallinity graphene via electrochemical exfoliation with molecular in situ encapsulation," Nanoscale **7**(37), 15362–15373 (2015).
[105]E. H. Joo *et al.*, "Electrochemically preparation of functionalized graphene using sodium dodecyl benzene sulfonate (SDBS)," Adv. Mater. Res. **747**, 246–249 (2013).
[106]J. P. Mensing *et al.*, "Facile preparation of graphene–metal phthalocyanine hybrid material by electrolytic exfoliation," J. Mater. Chem. **22**(33), 17094–17099 (2012).
[107]P. Khanra, T. Kuila, S. H. Bae, N. H. Kim, and J. H. Lee, "Electrochemically exfoliated graphene using 9-anthracene carboxylic acid for supercapacitor application," J. Mater. Chem. **22**(46), 24403–24410 (2012).
[108]N. Liu, F. Luo, H. Wu, Y. Liu, C. Zhang, and J. Chen, "One-step ionic-liquid-assisted electrochemical synthesis of ionic-liquid-functionalized graphene sheets directly from graphite," Adv. Funct. Mater. **18**(10), 1518–1525 (2008).
[109]S. Pei, Q. Wei, K. Huang, H.-M. Cheng, and W. Ren, "Green synthesis of graphene oxide by seconds timescale water electrolytic oxidation," Nat. Commun. **9**(1), 145 (2018).
[110]A. Ambrosi and M. Pumera, "Electrochemically exfoliated graphene and graphene oxide for energy storage and electrochemistry applications," Chem. Eur. J. **22**(1), 153–159 (2016).

[111]F. Zhou *et al.*, "Electrochemically scalable production of fluorine-modified graphene for flexible and high-energy ionogel-based microsupercapacitors," J. Am. Chem. Soc. **140**(26), 8198–8205 (2018).
[112]K. S. Rao, J. Senthilnathan, Y.-F. Liu, and M. Yoshimura, "Role of peroxide ions in formation of graphene nanosheets by electrochemical exfoliation of graphite," Sci. Rep. **4**(1), 4237 (2014).
[113]Z. Liu *et al.*, "Water-dispersed high-quality graphene: A green solution for efficient energy storage applications," ACS Nano **13**(8), 9431–9441 (2019).
[114]S. Yang *et al.*, "Ultrafast delamination of graphite into high-quality graphene using alternating currents," Angew. Chem. Int. Ed. **56**(23), 6669–6675 (2017).
[115]X. You, N. Liu, C. J. Lee, and J. J. Pak, "An electrochemical route to MoS_2 nanosheets for device applications," Mater. Lett. **121**, 31–35 (2014).
[116]N. Liu, P. Kim, J. H. Kim, J. H. Ye, S. Kim, and C. J. Lee, "Large-area atomically thin MoS_2 nanosheets prepared using electrochemical exfoliation," ACS Nano **8**(7), 6902–6910 (2014).
[117]A. Ambrosi, Z. Sofer, and M. Pumera, "Electrochemical exfoliation of layered black phosphorus into phosphorene," Angew. Chem. Int. Ed. **56**(35), 10443–10445 (2017).
[118]F. Li *et al.*, "Unlocking the electrocatalytic activity of antimony for CO_2 reduction by two-dimensional engineering of the bulk material," Angew. Chem. Int. Ed. **56**(46), 14718–14722 (2017).
[119]J. Yang *et al.*, "Free-standing black phosphorus thin films for flexible quasi-solid-state micro-supercapacitors with high volumetric power and energy density," ACS Appl. Mater. Interfaces **11**(6), 5938–5946 (2019).
[120]A. Ambrosi, Z. Sofer, J. Luxa, and M. Pumera, "Exfoliation of layered topological insulators Bi_2Se_3 and Bi_2Te_3 via electrochemistry," ACS Nano **10**(12), 11442–11448 (2016).
[121]S. Yang *et al.*, "Fluoride-free synthesis of two-dimensional titanium carbide (MXene) using a binary aqueous system," Angew. Chem. Int. Ed. **57**(47), 15491–15495 (2018).
[122]W. Wu, C. Zhang, L. Zhou, S. Hou, and L. Zhang, "High throughput synthesis of defect-rich MoS_2 nanosheets via facile electrochemical exfoliation for fast high-performance lithium storage," J. Colloid Interface Sci. **542**, 263–268 (2019).
[123]X. Pan *et al.*, "Electrochemically exfoliating MoS_2 into atomically thin planar-stacking through a selective lateral reaction pathway," Adv. Funct. Mater. **31**(8), 2007840 (2021).
[124]A. Kumar and P. K. Ahluwalia, "Electronic structure of transition metal dichalcogenides monolayers 1H-MX2 (M = Mo, W; X = S, Se, Te) from ab-initio theory: New direct band gap semiconductors," Eur. Phys. J. B **85**(6), 186 (2012).
[125]J. E. Padilha, H. Peelaers, A. Janotti, and C. G. Van de Walle, "Nature and evolution of the band-edge states in MoS_2: From monolayer to bulk," Phys. Rev. B **90**(20), 205420 (2014).
[126]H. Liu *et al.*, "Phosphorene: An unexplored 2D semiconductor with a high hole mobility," ACS Nano **8**(4), 4033–4041 (2014).
[127]H. Liu, Y. Du, Y. Deng, and P. D. Ye, "Semiconducting black phosphorus: Synthesis, transport properties and electronic applications," Chem. Soc. Rev. **44**(9), 2732–2743 (2015).
[128]L. Li *et al.*, "Direct observation of the layer-dependent electronic structure in phosphorene," Nat. Nanotechnol. **12**(1), 21–25 (2017).
[129]E. Gaufrès *et al.*, "Momentum-resolved dielectric response of free-standing mono-, bi-, and trilayer black phosphorus," Nano Lett. **19**(11), 8303–8310 (2019).
[130]M. Naguib *et al.*, "Two-dimensional nanocrystals produced by exfoliation of Ti_3AlC_2," Adv. Mater. **23**(37), 4248–4253 (2011).
[131]M. W. Barsoum, "The MN+1AXN phases: A new class of solids: Thermodynamically stable nanolaminates," Prog. Solid State Chem. **28**(1), 201–281 (2000).
[132]M. Naguib, V. N. Mochalin, M. W. Barsoum, and Y. Gogotsi, "25th anniversary article: MXenes: A new family of two-dimensional materials," Adv. Mater. **26**(7), 992–1005 (2014).
[133]M. Naguib *et al.*, "Two-dimensional transition metal carbides," ACS Nano **6**(2), 1322–1331 (2012).
[134]M. Alhabeb *et al.*, "Guidelines for synthesis and processing of two-dimensional titanium carbide ($Ti_3C_2T_x$ MXene)," Chem. Mater. **29**(18), 7633–7644 (2017).
[135]W. Sun *et al.*, "Electrochemical etching of Ti_2AlC to Ti_2CT_x (MXene) in low-concentration hydrochloric acid solution," J. Mater. Chem. A **5**(41), 21663–21668 (2017).
[136]T. Yin *et al.*, "Synthesis of $Ti_3C_2F_x$ MXene with controllable fluorination by electrochemical etching for lithium-ion batteries applications," Ceram. Int. **47**(20), 28642–28649 (2021).
[137]J. R. Dahn, R. Fong, and M. J. Spoon, "Suppression of staging in lithium-intercalated carbon by disorder in the host," Phys. Rev. B **42**(10), 6424–6432 (1990).
[138]Z. Zeng *et al.*, "Single-layer semiconducting nanosheets: High-yield preparation and device fabrication," Angew. Chem. Int. Ed. **50**(47), 11093–11097 (2011).
[139]W. Zhang, L. Sun, J. M. V. Nsanzimana, and X. Wang, "Lithiation/delithiation synthesis of few layer silicene nanosheets for rechargeable Li–O_2 Batteries," Adv. Mater. **30**(15), 1705523 (2018).
[140]Y. L. Zhong and T. M. Swager, "Enhanced electrochemical expansion of graphite for in situ electrochemical functionalization," J. Am. Chem. Soc. **134**(43), 17896–17899 (2012).
[141]Y. Yang *et al.*, "Electrochemically triggered graphene sheets through cathodic exfoliation for lithium ion batteries anodes," RSC Adv. **3**(36), 16130–16135 (2013).
[142]A. J. Cooper, N. R. Wilson, I. A. Kinloch, and R. A. W. Dryfe, "Single stage electrochemical exfoliation method for the production of few-layer graphene via intercalation of tetraalkylammonium cations," Carbon **66**, 340–350 (2014).
[143]Y. Zhang, Y. Xu, and R. Liu, "Regulating cations and solvents of the electrolyte for ultra-efficient electrochemical production of high-quality graphene," Carbon **176**, 157–167 (2021).
[144]S. Yang *et al.*, "A delamination strategy for thinly layered defect-free high-mobility black phosphorus flakes," Angew. Chem. Int. Ed. **57**(17), 4677–4681 (2018).
[145]J. Li *et al.*, "Ultrafast electrochemical expansion of black phosphorus toward high-yield synthesis of few-layer phosphorene," Chem. Mater. **30**(8), 2742–2749 (2018).
[146]J. Li *et al.*, "Printable two-dimensional superconducting monolayers," Nat. Mater. **20**(2), 181–187 (2021).
[147]M. H. Dalal, C.-Y. Lee, and G. G. Wallace, "Cathodic exfoliation of graphite into graphene nanoplatelets in aqueous solution of alkali metal salts," J. Mater. Sci. **56**(4), 3612–3622 (2021).
[148]S. García-Dalí *et al.*, "Aqueous cathodic exfoliation strategy toward solution-processable and phase-preserved MoS_2 nanosheets for energy storage and catalytic applications," ACS Appl. Mater. Interfaces **11**(40), 36991–37003 (2019).
[149]M. Zhou, J. Tang, Q. Cheng, G. Xu, P. Cui, and L.-C. Qin, "Few-layer graphene obtained by electrochemical exfoliation of graphite cathode," Chem. Phys. Lett. **572**, 61–65 (2013).
[150]Y. Yang, F. Lu, Z. Zhou, W. Song, Q. Chen, and X. Ji, "Electrochemically cathodic exfoliation of graphene sheets in room temperature ionic liquids N-butyl, methylpyrrolidinium bis(trifluoromethylsulfonyl)imide and their electrochemical properties," Electrochim. Acta **113**, 9–16 (2013).
[151]I. Jeon, B. Yoon, M. He, and T. M. Swager, "Hyperstage graphite: Electrochemical synthesis and spontaneous reactive exfoliation," Adv. Mater. **30**(3), 1704538 (2018).
[152]Z. Lin *et al.*, "Solution-processable 2D semiconductors for high-performance large-area electronics," Nature **562**(7726), 254–258 (2018).
[153]P. Zhang *et al.*, "Electrochemically exfoliated high-quality 2H-MoS_2 for multi-flake thin film flexible biosensors," Small **15**(23), 1901265 (2019).
[154]W. Yu *et al.*, "Chemically exfoliated VSe_2 monolayers with room-temperature ferromagnetism," Adv. Mater. **31**(40), 1903779 (2019).
[155]L. Lu *et al.*, "Broadband nonlinear optical response in few-layer antimonene and antimonene quantum dots: A promising optical Kerr media with enhanced stability," Adv. Opt. Mater. **5**(17), 1700301 (2017).
[156]Z. Huang, H. Hou, Y. Zhang, C. Wang, X. Qiu, and X. Ji, "Layer-tunable phosphorene modulated by the cation insertion rate as a sodium-storage anode," Adv. Mater. **29**(34), 1702372 (2017).
[157]M. Mao, M. Wang, J. Hu, G. Lei, S. Chen, and H. Liu, "Simultaneous electrochemical synthesis of few-layer graphene flakes on both electrodes in protic ionic liquids," Chem. Commun. **49**(46), 5301–5303 (2013).

[158]J. C. Bradley, J. Crawford, K. Ernazarova, M. McGee, and S. G. Stephens, "Wire formation on circuit boards using spatially coupled bipolar electrochemistry," Adv. Mater. **9**(15), 1168–1171 (1997) (in English).
[159]S. E. Fosdick, K. N. Knust, K. Scida, and R. M. Crooks, "Bipolar electrochemistry," Angew. Chem. Int. Ed. **52**(40), 10438–10456 (2013).
[160]N. Shida, Y. Zhou, and S. Inagi, "Bipolar electrochemistry: A powerful tool for electrifying functional material synthesis," Acc. Chem. Res. **52**(9), 2598–2608 (2019).
[161]F. Mavré *et al.*, "Bipolar electrodes: A useful tool for concentration, separation, and detection of analytes in microelectrochemical systems," Anal. Chem. **82**(21), 8766–8774 (2010).
[162]J. F. L. Duval, G. K. Huijs, W. F. Threels, J. Lyklema, and H. P. van Leeuwen, "Faradaic depolarization in the electrokinetics of the metal–electrolyte solution interface," J. Colloid Interface Sci. **260**(1), 95–106 (2003).
[163]J. F. L. Duval, M. Minor, J. Cecilia, and H. P. van Leeuwen, "Coupling of lateral electric field and transversal faradaic processes at the conductor/electrolyte solution interface," J. Phys. Chem. B **107**(17), 4143–4155 (2003).
[164]J. F. L. Duval, J. Buffle, and H. P. van Leeuwen, "Quasi-reversible Faradaic depolarization processes in the electrokinetics of the metal/solution interface," J. Phys. Chem. B **110**(12), 6081–6094 (2006).
[165]A. Allagui, M. A. Abdelkareem, H. Alawadhi, and A. S. Elwakil, "Reduced graphene oxide thin film on conductive substrates by bipolar electrochemistry," Sci. Rep. **6**(1), 21282 (2016).
[166]A. Allagui, J. M. Ashraf, M. Khalil, M. A. Abdelkareem, A. S. Elwakil, and H. Alawadhi, "All-solid-state double-layer capacitors using binderless reduced graphene oxide thin films prepared by bipolar electrochemistry," ChemElectroChem **4**(8), 2084–2090 (2017).
[167]I. Khakpour, A. Rabiei Baboukani, A. Allagui, and C. Wang, "Bipolar exfoliation and in situ deposition of high-quality graphene for supercapacitor application," ACS Appl. Energy Mater. **2**(7), 4813–4820 (2019).
[168]E. T. Bjerglund, M. E. P. Kristensen, S. Stambula, G. A. Botton, S. U. Pedersen, and K. Daasbjerg, "Efficient graphene production by combined bipolar electrochemical intercalation and high-shear exfoliation," ACS Omega **2**(10), 6492–6499 (2017).
[169]C. C. Mayorga-Martinez, B. Khezri, A. Y. S. Eng, Z. Sofer, P. Ulbrich, and M. Pumera, "Bipolar electrochemical synthesis of WS_2 nanoparticles and their application in magneto-immunosandwich assay," Adv. Funct. Mater. **26**(23), 4094–4098 (2016).
[170]C. C. Mayorga-Martinez, N. Mohamad Latiff, A. Y. S. Eng, Z. Sofer, and M. Pumera, "Black phosphorus nanoparticle labels for immunoassays via hydrogen evolution reaction mediation," Anal. Chem. **88**(20), 10074–10079 (2016).
[171]R. J. Toh, C. C. Mayorga-Martinez, Z. Sofer, and M. Pumera, "$MoSe_2$ Nanolabels for electrochemical immunoassays," Anal. Chem. **88**(24), 12204–12209 (2016).
[172]Y. Wang, C. C. Mayorga-Martinez, X. Chia, Z. Sofer, and M. Pumera, "Nonconductive layered hexagonal boron nitride exfoliation by bipolar electrochemistry," Nanoscale **10**(15), 7298–7303 (2018).
[173]M. Armand and J. M. Tarascon, "Building better batteries," Nature **451**(7179), 652–657 (2008).
[174]Y. L. Liang and Y. Yao, "Positioning organic electrode materials in the battery landscape," Joule **2**, 1690–1706 (2018).
[175]J. X. Nan *et al.*, "Nanoengineering of 2D MXene-based materials for energy storage applications," Small **17**(9), 1902085 (2021).
[176]A. Jamaluddin, B. Umesh, F. M. Chen, J. K. Chang, and C. Y. Su, "Facile synthesis of core-shell structured Si at graphene balls as a high-performance anode for lithium-ion batteries," Nanoscale **12**(17), 9616–9627 (2020) (in English).
[177]Z. H. Sun *et al.*, "A practical Li-ion full cell with a high-capacity cathode and electrochemically exfoliated graphene anode: Superior electrochemical and low-temperature performance," ACS Appl. Energy Mater. **2**(1), 486–492 (2019).
[178]D. L. Vu, Y. J. Kwon, S. C. Lee, J. U. Lee, and J. W. Lee, "Exfoliated graphene nanosheets as high-power anodes for lithium-ion batteries," Carbon Lett. **29**(1), 81–87 (2019) (in English).
[179]G. Wang *et al.*, "Vertically aligned MoS_2 nanosheets patterned on electrochemically exfoliated graphene for high-performance lithium and sodium storage," Adv. Energy Mater. **8**(8), 1702254 (2018).
[180]T. N. J. I. Edison *et al.*, "Electrochemically exfoliated graphene sheets as electrode material for aqueous symmetric supercapacitors," Surf. Coat. Technol. **416**, 127150 (2021).
[181]J.-K. Chih, A. Jamaluddin, F. Chen, J.-K. Chang, and C.-Y. Su, "High energy density of all-screen-printable solid-state microsupercapacitors integrated by graphene/CNTs as hierarchical electrodes," J. Mater. Chem. A **7**(20), 12779–12789 (2019).
[182]A. A. B. Hamra, H. N. Lim, W. K. Chee, and N. M. Huang, "Electro-exfoliating graphene from graphite for direct fabrication of supercapacitor," Appl. Surf. Sci. **360**, 213–223 (2016).
[183]T. Huang *et al.*, "Boosting capacitive sodium-ion storage in electrochemically exfoliated graphite for sodium-ion capacitors," ACS Appl. Mater Interfaces **12**(47), 52635–52642 (2020).
[184]M. Jing, T. Wu, Y. Zhou, X. Li, and Y. Liu, "Nitrogen-doped graphene via in-situ alternating voltage electrochemical exfoliation for supercapacitor application," Front. Chem. Original Res. **8**, 428 (2020) (in English).
[185]R. N. Muthu and S. S. V. Tatiparti, "Electrode and symmetric supercapacitor device performance of boron-incorporated reduced graphene oxide synthesized by electrochemical exfoliation," Energy Storage **2**(4), e134 (2020).
[186]R. Hu, Z. Huang, B. Wang, H. Qiao, and X. Qi, "Electrochemical exfoliation of molybdenum disulfide nanosheets for high-performance supercapacitors," J. Mater. Sci.-Mater. Electron. **32**(6), 7237–7248 (2021).
[187]F. Li *et al.*, "Advanced composite 2D energy materials by simultaneous anodic and cathodic exfoliation," Adv. Energy Mater. **8**(12), 1702794 (2018).
[188]S. Mukherjee *et al.*, "Exfoliated transition metal dichalcogenide nanosheets for supercapacitor and sodium ion battery applications," R. Soc. Open Sci. **6**(8), 190437 (2019).
[189]J. W. Yan *et al.*, "Multilayer graphene sheets converted directly from anthracite in the presence of molten iron and their applications as anode for lithium ion batteries," Synth. Met. **263**, 116364 (2020) (in English).
[190]Y. Yang, S. Leng, and W. Shi, "Electrochemical exfoliation of porous antimonene as anode materials for sodium-ion batteries," Electrochem. Commun. **126**, 107025 (2021).
[191]C. Shen *et al.*, "Bismuthene from sonoelectrochemistry as a superior anode for potassium-ion batteries," J. Mater. Chem. A **8**(1), 453–460 (2020).
[192]L. He *et al.*, "Electrochemical exfoliation and functionalization of black phosphorene to enhance mechanical properties and flame retardancy of waterborne polyurethane," Composites, Part B **202**, 108446 (2020).
[193]L. Mei *et al.*, "Simultaneous electrochemical exfoliation and covalent functionalization of MoS_2 membrane for ion sieving," Adv. Mater. **34**(26), 2201416 (2022).
[194]D. Alliata, R. Kötz, O. Haas, and H. Siegenthaler, "In situ AFM study of interlayer spacing during anion intercalation into HOPG in aqueous electrolyte," Langmuir **15**(24), 8483–8489 (1999).
[195]F. P. Campana, H. Buqa, P. Novák, R. Kötz, and H. Siegenthaler, "In situ atomic force microscopy study of exfoliation phenomena on graphite basal planes," Electrochem. Commun. **10**(10), 1590–1593 (2008).
[196]Z. Xia, V. Bellani, J. Sun, and V. Palermo, "Electrochemical exfoliation of graphite in H_2SO_4, Li_2SO_4 and $NaClO_4$ solutions monitored in situ by Raman microscopy and spectroscopy," Faraday Discuss. **227**, 291–305 (2021).